

Direct partitioning of eddy-covariance water and carbon dioxide fluxes into ground and plant components

Einara Zahn^a, Elie Bou-Zeid^{*,a}, Stephen P. Good^b, Gabriel G. Katul^c, Christoph K. Thomas^d, Khaled Ghannam^e, James A. Smith^a, Marcelo Chamecki^f, Nelson L. Dias^g, Jose D. Fuentes^h, Joseph G. Alfieriⁱ, Hyojung Kwon^j, Kelly K. Caylor^{k,l}, Zhiqiu Gao^{m,n}, Keir Soderberg^o, Nicolas E. Bambach^p, Lawrence E. Hipps^q, John H. Prueger^r, William P. Kustasⁱ

^a Department of Civil and Environmental Engineering, Princeton University, Princeton, New Jersey, USA

^b Department of Biological and Ecological Engineering, Oregon State University, Corvallis, OR 97331, USA

^c The Department of Civil and Environmental Engineering, Duke University, Durham, North Carolina 27708, USA

^d Micrometeorology Group and Bayreuth Center of Ecology and Environmental Research, University of Bayreuth, Bayreuth, Germany

^e Program in Atmospheric and Oceanic Sciences (Cooperative Institute for Modeling the Earth System), Princeton University, Princeton NJ, USA

^f Department of Atmospheric & Oceanic Sciences, University of California in Los Angeles, Los Angeles, California, USA

^g Department of Environmental Engineering, Federal University of Paraná, Curitiba, PR, Brazil

^h Department of Meteorology and Atmospheric Science, Penn State University, University Park, PA 16802, USA

ⁱ USDA-ARS, Hydrology and Remote Sensing Lab, Beltsville, MD 20705-2350, USA

^j Department of Forest Ecosystems and Society, Oregon State University, Corvallis, OR 97333, USA

^k Department of Geography, University of California Santa Barbara, Santa Barbara, CA 93016, United States of America

^l Earth Research Institute, University of California, Santa Barbara, Santa Barbara, CA 93016, United States of America

^m Nanjing University of Information Science and Technology, Nanjing 210044, China

ⁿ Institute of Atmospheric Physics, Chinese Academy of Sciences, Beijing 100029, China

^o Geochemistry, S.S. Papadopoulos & Associates, Inc., Rockville, Maryland

^p Department of Land, Air and Water Resources, University of California, Davis

^q Plants, Soils and Climate Department, Utah State University, Logan, UT 84322-4820, USA

^r National Laboratory for Agriculture and the Environment, USDA ARS, Ames, IA 50011, USA

ARTICLE INFO

ABSTRACT

Keywords:

Carbon dioxide fluxes
Eddy Covariance
Evapotranspiration
Flux partitioning
Photosynthesis
Respiration

The partitioning of evapotranspiration (ET) into surface evaporation (E) and stomatal-based transpiration (T) is essential for analyzing the water cycle and earth surface energy budget. Similarly, the partitioning of net ecosystem exchange (NEE) of carbon dioxide into respiration (R) and photosynthesis (P) is needed to quantify the controls on its sources and sinks. Promising approaches to obtain these components from field measurements include partitioning models based on analysis of conventional high frequency eddy-covariance data. Here, two such existing approaches, based on similarity between non-stomatal (R and E) and stomatal (P and T) components, are considered: the Modified Relaxed Eddy Accumulation (MREA) and Flux-Variance Similarity (FVS) models. Moreover, a simpler technique is proposed based on a Conditional Eddy-Covariance (CEC) scheme. All approaches were evaluated against independent estimates of transpiration and respiration. The CEC method agreed better with measurements of transpiration over a grass field, with a smaller root mean square error (5.9 W m^{-2}) and higher correlation (0.96). At a forest site, better agreement with soil respiration was found for FVS above the canopy, while CEC and MREA performed better below the canopy. Further application of these methods over a vineyard and a pine forest across different seasons provided insight into the main strengths and weaknesses of each approach. FVS and MREA converge less often when ground flux components dominate, while CEC might result in noisy P and R for small NEE . Finally, in the CEC and MREA framework, the ratio T/ET is shown to be related to the correlation coefficient for carbon dioxide and water vapor concentrations, which can thus be used as a qualitative measure of the importance of stomatal and non-stomatal components. Overall, these results advance the understanding of the skill and agreement of all three methods, and inform future studies where the various approaches can be applied simultaneously and intercompared.

* Corresponding author.

E-mail address: ebouzeid@princeton.edu (E. Bou-Zeid).

1. Introduction

The total evapotranspiration (ET) is composed of transpiration (T), defined as water flowing through plants, and evaporation (E) from soil and other surfaces. While ET is essential in studies of water and energy budgets, the characterization of its individual components is often required, e.g. when assessing limitations to ecosystem services. For instance, T is usually associated with plant productivity, and this flux can be used to improve irrigation practices and crop management (Peddinti and Kambhammettu, 2019; Sun et al., 2019). Similarly, the carbon dioxide flux (F_c) measured above canopies is the net flux composed of plant photosynthesis (P), which is directly related to transpiration, and respiration from soil (R) and other above-ground biomass components.

A practical barrier to flux partitioning is that the most common method to measure water and carbon fluxes, the eddy-covariance (EC) approach, only provides the total net fluxes. As a result, much remains to be improved and understood regarding partitioning methods for both ET and F_c . Advancement in this area is becoming increasingly necessary for understanding the controls on water and carbon fluxes at multiple spatial scales. For instance, it would improve calibration and validation of satellite-derived fluxes and of land-atmosphere interaction schemes in Earth system models (Stoy et al., 2019; Sun et al., 2019; Wang et al., 2016).

Given the importance of the subject, various partitioning techniques have been proposed in the last few decades. A detailed review of current available methods for ET partitioning, some of which can also be applied to F_c , is provided elsewhere (Kool et al., 2014). In certain cases, one of the ET components can be measured independently of the eddy-covariance method. For example, sap-flux (Kostner et al., 2017) and chamber measurements (Koskinen et al., 2014; Thomas et al., 2013) can be employed, respectively, to determine transpiration and soil respiration/evaporation. When coupled with total fluxes obtained by the EC approach, the other components can then be inferred by assuming a simple budget equation, although any error in the determination of one component will be mirrored with an opposite sign in the other component computed as a residual. An even simpler approach using below- and above-canopy ET and F_c measurements to infer all four components has also been used (Ma et al., 2020; Misson et al., 2007; Paul-Limoges et al., 2017; 2020; Rousard et al., 2006; Wilson and Meyers, 2001). Although not a direct method, another technique that has been gaining popularity consists of partitioning both ET and F_c by discriminating the isotopic signatures related to CO_2 and H_2O from each source and sink (Good et al., 2014; Lee et al., 2020; WIchura et al., 2017). While all of these approaches have been improved in the last decade or so, most of them still require laborious measurements and/or expensive sensors, which prevents their implementation over a broad range of ecosystems. In addition, even direct measurements still require parameterizations and physical assumptions, all of which can potentially add uncertainties to flux estimates.

Because of the general similarity between sources and sinks of the different components of F_c and ET , and given their simultaneous measurements by the same instruments in EC systems, previous studies developed partitioning methods of EC fluxes into their individual components. The level of complexity of recently proposed methods (Li et al., 2019; Nelson et al., 2018; Scanlon and Sahu, 2008; Scott and Biederman, 2017; Thomas et al., 2008; Wei et al., 2017; Zhou et al., 2016) ranges from machine learning approaches (Nelson et al., 2018) and optimization models (Perez-Priego et al., 2018) to regression models (Reichstein et al., 2005; Scott and Biederman, 2017; Zhou et al., 2016). Nonetheless, independent of the complexity of the model, some of these approaches may require knowledge of various environmental variables (e.g., soil temperature), as well as canopy and plant characteristics (e.g., leaf area index and plant conductance), or even variables that are difficult to measure at the scale of interest such as water-use efficiency (WUE). Furthermore, a subset of these methods (Li et al., 2019; Nelson et al.,

2018; Scott and Biederman, 2017; Zhou et al., 2016) rely on prior knowledge of the two carbon dioxide flux components, which already has its own uncertainty. In such formulations, gross primary productivity (GPP) is a required input variable, to be later related to WUE . These additional requirements prevent the implementation in sites without such information or measurements, and add uncertainties when these inputs are unavailable and need to be parameterized. In this regard, simpler models that only require commonly measured variables offer many advantages.

Such simpler models have been proposed to partition both ET and F_c components based on the use of high-frequency turbulence data from EC systems. Their first assumption is that the transpiration and photosynthesis (stomatal T and P) share the same sources and sinks, which are distinct from those of evaporation and respiration (non-stomatal E and R). Subsequently, these approaches postulate that both H_2O and CO_2 can be treated as passive scalars, with similar turbulent Schmidt numbers, and are thus transported similarly by turbulence from a given source (plants or soils). Such formulations not only reduce the complexity of the model, but also decrease or eliminate the need for external variables such as GPP or WUE , although the latter is still needed in some of these approaches. Furthermore, they allow simultaneous partitioning of both carbon and water vapor components. To this end, two models were previously proposed (Scanlon and Sahu, 2008; Thomas et al., 2008), and will be described in detail in Section 2. The method developed by Thomas et al. (2008) combines octant analysis and the relaxed eddy accumulation technique, and is here called Modified Relaxed Eddy Accumulation (MREA), while the first approach (Scanlon and Kustas, 2010; Scanlon and Sahu, 2008) is based on Flux-Variance Similarity, and is here referred to as the FVS method.

Many studies have investigated the performance of FVS (Klosterhalfen et al., 2019a; 2019b; Peddinti and Kambhammettu, 2019; Rana et al., 2018; Scanlon et al., 2019; Sulman et al., 2016; Wang et al., 2016) and, to a lesser extent the performance of MREA (Klosterhalfen et al., 2019a; 2019b; Thomas et al., 2013), over different ecosystems. The challenge, which is common to all partitioning studies, is how to evaluate their results. While independent and reliable estimates of E and T are rarely available at the scale of interest, comparing different techniques that are premised on different assumptions may be viewed as a logical first step. When these techniques agree, the confidence in the component-wise inferred fluxes is increased. However, a recent comparison of MREA and FVS (Klosterhalfen et al., 2019a) across many sites showed variable agreement, not only between the two methods, but also relative to independent measurements and parameterizations of soil respiration and evaporation. At present, it remains unclear what is causing divergence or agreement between the methods.

One shortcoming of the FVS method is that it requires an a priori estimate of ecosystem water-use efficiency. The usual lack of WUE measurements then necessitates its parameterization. The most common formulation requires the intercellular carbon dioxide concentration, for which many models are available (Katul et al., 2000). However, it has been shown that the results of the FVS method are sensitive to WUE (Scanlon et al., 2019; Skaggs et al., 2018). In addition, FVS does not converge to realistic solutions in many situations (Skaggs et al., 2018), which may lead to biases in the integrated results of mean ecosystem exchanges of water vapor and carbon dioxide. The MREA method, on the other hand, has been less explored. Nonetheless, the study by Klosterhalfen et al. (2019a) indicated that the method has a tendency to underestimate soil components.

The similarity between stomatal and non-stomatal pathways for H_2O and CO_2 exchanges is further exploited here to offer another partitioning approach for ET and F_c that is solely based on eddy-covariance data. This new proposed method, hereafter referred to as Conditional Eddy Covariance (CEC), is evaluated along with FVS and MREA, against independent E and T estimates obtained over an irrigated grass field using leaf-level measurements, and against soil respiration measured at a pine forest. The predictions of all three models are then compared over two

additional sites across seasons: a vineyard and a sparse forest. The aim is to address the following questions:

1. When do partitioning approaches solely based on eddy-covariance data provide biophysically meaningful results over different ecosystems?
2. How do estimates from CEC compare to those from previously developed methods (FVS and MREA), and under which conditions do they agree?
3. Which assumptions limit the validity of these models and what experimental design considerations are important when collecting measurements for their application?

2. Description of partitioning methods

A description of the previous partitioning methods (FVS and MREA) is provided to establish their assumptions. The newly proposed method, the CEC approach, is then developed. All three methods can be implemented to obtain simultaneous non-stomatal (respiration and evaporation) and stomatal (photosynthesis and transpiration) components during the day. Note that the term we here call “photosynthesis” represents a net photosynthesis, which is carboxylation minus photorespiration and leaf respiration (see the discussion of Wohlfahrt and Gu (2015) about different definitions of photosynthesis). The non-stomatal component may also comprise stem respiration, in addition to ground respiration. Note that none of the methods is able to distinguish between autotrophic respiration from the plant roots and heterotrophic respiration.

While we do not expect significant photosynthesis and transpiration during nighttime hours in the ecosystems studied here, CEC and MREA can still be applied during these periods. This is possible because their formulations do not require a measure of water-use efficiency. Under such conditions, ideally, both methods would indicate $F_c = R$ and $ET = E$.

2.1. Nomenclature

Throughout, the following nomenclature is used: a Cartesian coordinate system is defined with x along the mean wind direction, y along the lateral direction, and z along the vertical direction with $z = 0$ being the ground or forest floor (positive upwards). The instantaneous velocity components along x, y, z are designated as u, v, w , respectively, while CO_2 and H_2O concentrations are designated as c and q . Instantaneous flow variables are decomposed into a time-averaged (indicated by overlines) and fluctuating (indicated by primes) quantities. All flows are assumed to be stationary and horizontally homogeneous. The coordinate system here is selected so that $\bar{v} = \bar{w} = 0$. For an arbitrary scalar $s = \bar{s} + s'$ with root-mean squared fluctuations $\sigma_s = (\bar{s}^2)^{1/2}$, the mean mass balance reduces to

$$\frac{\partial \bar{s}}{\partial t} = 0 = -\frac{\partial F(z)}{\partial z} + S_v, \quad (1)$$

where t is time; $F(z)$ is the total vertical flux of the scalar; and S_v are net sources (positive) and sinks (negative) from the vegetation volume. Upon integrating this expression from $z = 0$ to the measurement height z_m above the canopy we obtain

$$\overline{w's'}(z_m) = F_s(0) + \int_0^{z_m} S_v(z) dz, \quad (2)$$

where $\overline{w's'}(z_m)$ is the turbulent flux measured by the EC method at height z_m and assumed to dominate over its molecular counterpart at z_m due to the high Reynolds number at that height; $F_s(0)$ is the ground flux (ground evaporation or respiration when $s = q$ or $s = c$, respectively); $\int_0^{z_m} S_v(z) dz$ is the integral of net sources or sinks, transpiration and

photosynthesis, within the canopy volume. The partitioning methods to be discussed next seek to partition $\overline{w's'}(z_m)$ into its two components: stomatal canopy fluxes and non-stomatal fluxes, the latter being mainly from the ground but with contributions from stem respiration and evaporation.

2.2. Flux-variance similarity (FVS) method

The derivation of the FVS method starts by decomposing the high-frequency time series of carbon and water vapor into their stomatal (c_p and q_t , related to photosynthesis and transpiration) and non-stomatal components (c_r and q_e , related to respiration and evaporation) (Scanlon and Kustas, 2010; Scanlon and Sahu, 2008). The budget equations for their variances and fluxes are then manipulated and related to a flux-based water-use efficiency ($WUE = P/T$) in terms of the slope between the fluctuations q'_t and c'_p ($c'_p = WUE q'_t$). The final equations for the flux components take the following form

$$\frac{E_{\text{FVS}}}{T_{\text{FVS}}} = -\rho_{c_p, c_r}^2 + \rho_{c_p, c_r}^2 \sqrt{1 - \rho_{c_p, c_r}^{-2} \left(1 - WUE^2 \frac{\sigma_q^2}{\sigma_{c_p}^2} \right)}, \quad (3a)$$

$$\frac{R_{\text{FVS}}}{P_{\text{FVS}}} = -\rho_{c_p, c_r}^2 \pm \rho_{c_p, c_r}^2 \sqrt{1 - \rho_{c_p, c_r}^{-2} \left(1 - \frac{\sigma_c^2}{\sigma_{c_p}^2} \right)}, \quad (3b)$$

where ρ_{c_p, c_r} is the correlation coefficient between c_p and c_r ; σ_c and σ_q are the standard deviations of carbon dioxide and water vapor concentration fluctuations, respectively; and σ_{c_p} is the standard deviation of carbon dioxide fluctuations that are related to photosynthesis. Two complementary equations (shown in Appendix A) are also derived to compute ρ_{c_p, c_r} and σ_{c_p} . More recently, Scanlon et al. (2019) derived the following conditions to obtain physically meaningful fluxes ($P \leq 0$ and $R, T, E \geq 0$),

$$\rho_{c,q}^{-1} \frac{\sigma_c}{\sigma_q} \leq \frac{\overline{w'c'}}{\overline{w'q'}} < \rho_{c,q} \frac{\sigma_c}{\sigma_q} \quad \text{for } \rho_{c,q} < 0, \text{ and} \quad (4a)$$

$$\frac{\overline{w'c'}}{\overline{w'q'}} < \rho_{c,q} \frac{\sigma_c}{\sigma_q} \quad \text{for } \rho_{c,q} > 0. \quad (4b)$$

As noted in previous studies (Klosterhalfen et al., 2019b; Scanlon et al., 2019), one of the main sources of uncertainty in the FVS method arises from approximations used to represent the correlation coefficient between carbon components (ρ_{c_r, c_p}) and water vapor components (ρ_{q_t, q_e}). Using synthetic time series from large eddy simulations (LES), Klosterhalfen et al. (2019b) determined multiplicative constants to correct these approximations, which improved the performance of the method. However, it is not possible to obtain such correction factors when dealing with field measurements, or to ascertain the applicability of LES determined ones. Therefore, no corrections are applied in our implementation of the method, and uncertainties regarding this approximation thus remain.

The only variable not directly obtained from eddy-covariance measurements is the water-use efficiency, usually parameterized as

$$WUE = 0.65 \frac{\overline{c_c} - \overline{c_s}}{\overline{q_c} - \overline{q_s}}, \quad (5)$$

where $\overline{q_c}$ and $\overline{c_c}$ are H_2O and CO_2 atmospheric mean concentrations near the canopy, while $\overline{q_s}$ and $\overline{c_s}$ are the mean intercellular concentrations. The factor 0.65 originates from the ratio of molecular diffusivities of CO_2 to H_2O . The near-canopy concentrations are found using the logarithmic profile (and using mean concentrations from EC data), while $\overline{q_s}$ is calculated by assuming stomatal saturation and that the leaf temperature is the same as the air temperature (well-coupled leaf). The largest source of uncertainty in this model is the computation of $\overline{c_s}$. Here, we test different models for $\overline{c_s}$ (described in Appendix A),

obtaining different estimates for all four components. Therefore, for each 30-minute time interval we end up with up to five different values for T_{FVS} , one for each parameterization of \bar{c}_s . To facilitate comparison with the other two methods, and to maximize the number of 30-minute time intervals with available solution for the FVS method, we compute the ensemble average of all valid T_{FVS} estimates (same for other components) found by the method for each 30-min interval.

2.3. Modified relaxed eddy accumulation (MREA) method

The MREA is a combination of the relaxed eddy accumulation (Baker, 2000; Katul et al., 1996; Pattey et al., 1993) and conditional sampling based on multi-scalar octant analysis (Dettori et al., 2008; Scanlon and Albertson, 2001). The method relies on the assumption of similarity of turbulent transport of non-stomatal components from the soil. It selects from ejections (defined by $w' > 0$) only those which are enriched in both carbon ($c' > 0$) and water vapor ($q' > 0$), defining the first octant (O1) of an octant analysis between the three variables (Scanlon and Albertson, 2001). The derivation is presented elsewhere (Thomas et al., 2008) and is not repeated here.

Using only statistics obtained from EC data, respiration is computed by the following expression

$$R_{\text{MREA}} = \beta \sigma_w \frac{\sum_{i=1}^N I_H c'}{\sum_{i=1}^N I_{H,w+}}, \quad (6)$$

where σ_w is the standard deviation of vertical velocity and N is the total number of points in the time series. Furthermore, β is a similarity constant computed as $\beta = \sigma_w / (\bar{w}_+ - \bar{w}_-)$ (Baker et al., 1992; Katul et al., 1994), where \bar{w}_+ and \bar{w}_- are the mean vertical velocities in updrafts and downdrafts, respectively. To avoid sampling points close to the origin that are possibly related to transpiration and photosynthesis, a hyperbolic threshold H may be introduced (Thomas et al., 2008) leading to the following indicator functions I_H and $I_{H,w+}$

$$I_H = \begin{cases} 1 & \text{if } w' > 0, c' > 0, q' > 0, \left| \frac{c'}{\sigma_c} \right| > \left| \frac{H\sigma_q}{q'} \right| \\ 0 & \text{otherwise} \end{cases} \quad (7a)$$

$$I_{H,w+} = \begin{cases} 1 & \text{if } w' > 0, \left| \frac{q'}{\sigma_q} \right| > \left| \frac{H\sigma_c}{c'} \right|, \left| \frac{c'}{\sigma_c} \right| > \left| \frac{H\sigma_q}{q'} \right| \\ 0 & \text{otherwise.} \end{cases} \quad (7b)$$

An expression for evaporation E_{MREA} can be found by substituting c' by q' in Eq. (6), thereby allowing both non-stomatal components to be directly computed from EC measurements. The stomatal transpiration and photosynthesis components are then found as the residuals from the total ET and F_c . This formulation might result in negative transpiration if $E_{\text{MREA}} > ET$. In such cases, overestimation of respiration may also be expected during periods when photosynthesis is known to be negligible, characterized by R_{MREA} larger than F_c . Thus, we only consider solutions for both ET and F_c components to be biophysically meaningful when $E_{\text{MREA}} < ET$ was satisfied. We also added an additional constraint regarding the number of points in the first (O1: $w' > 0, q' > 0, c' > 0$) and second (O2: $w' > 0, q' > 0, c' < 0$) octants. Based on analyses conducted with the MREA and CEC method (introduced in Section 2.4), we require that at least 20% of the total number of points be present in these two octants. Furthermore, MREA is only applied if at least 5% of the points are in O1; otherwise, we assume that ground flux components are negligible and attribute all fluxes to T_{MREA} and P_{MREA} (more details about these constraints are presented in Section 2.4).

Thomas et al. (2008) evaluated the MREA method against independent estimates of soil respiration and found that $H = 0.25$ resulted in the best match between estimates. In our tests, we verified that MREA was no longer very sensitive to H when the new constraint $E_{\text{MREA}} > ET$ on R_{MREA} was imposed. Thus, we did not use a hyperbolic threshold in the

present analyses, i.e., $H = 0$.

2.4. A new partitioning approach: The conditional eddy covariance (CEC) method

The main motivation of this approach is to continue to exploit the assumption of transport similarity between stomatal and non-stomatal pairs, while circumventing the need for WUE and GPP. While the basic idea was reported in Thomas et al. (2008, see their Eqs. 1 & 2), it was not developed further. Similar to MREA, CEC uses the information carried by ejections to represent the signature of the surface. As described in Section 2.3, the MREA method computes respiration (or evaporation) directly from the first octant, i.e., the method assumes that the covariance or relaxed eddy accumulation method applied to the fluctuations following conditions (7b) yields the soil flux component. CEC diverges from MREA in this latter part: we consider that the covariances computed from O1 (defined in the same way as for MREA) are conditional statistics, f_E and f_R , that only characterize the non-stomatal components of water vapor and carbon dioxide, respectively. In other words, these covariances are akin to “sample” fluxes that represent, but are not equal to, the respective soil components. To represent canopy fluxes, we additionally include information from the second octant (O2), from which we compute conditional covariances representing transpiration f_T and photosynthesis f_P (Fig. 1 shows a conceptual framework of the method). These sample fluxes are obtained by the covariance of both scalars with the vertical velocity for ejections only, conditioned on the respective octant. For example, f_E and f_T are given as

$$f_E = \frac{1}{N} \sum I_E w' q' \quad \text{and} \quad f_T = \frac{1}{N} \sum I_T w' q' \quad (8)$$

where I_E and I_T are indicator functions given by

$$I_E = \begin{cases} 1 & \text{if } c' > 0, w' > 0, q' > 0 \\ 0 & \text{otherwise} \end{cases} \quad (9a)$$

$$I_T = \begin{cases} 1 & \text{if } c' < 0, w' > 0, q' > 0 \\ 0 & \text{otherwise.} \end{cases} \quad (9b)$$

Limiting these sample fluxes to $w' > 0$ serves to only interrogate the ejections, which should carry the signature of surface fluxes, as opposed to sweeps (Thomas et al., 2008, see their Fig. 3). It is also well established that the skewness of w' is positive above vegetated canopies (Poggi et al., 2004); therefore, large perturbations in w' are likely to be associated with ejective motion. Furthermore, ejections that are depleted in water vapor (regardless of their c') are assumed to be associated with air parcels that are swept to the surface from aloft, but do not interact with the surface (or canopy) for a time long enough to capture an evaporation or transpiration signal. These events are thus excluded in the computation of the ratios, but included in the computation of the total eddy covariance fluxes where they do contribute (negatively or counter to the gradient) to the total. We also conducted tests where these events were included, with a minimal impact on the results. We additionally tested the method with a hyperbolic threshold H and found that the results were not sensitive to the choice of H ; therefore, we did not include such a threshold. Following the steps above, similar expressions are then obtained for CO_2 (f_R and f_P) by substituting q' by c' in Eq. 8. Note that the indicator functions I_R and I_P remain the same as I_E and I_T , respectively.

The next step is to define a ratio of the sample fluxes, and this ratio is then assumed equal to the ratio of the total stomatal and non-stomatal fluxes from all octants

$$r_{ET} = \frac{f_E}{f_T} = \frac{E}{T} \quad \text{and} \quad r_{Fc} = \frac{f_R}{f_P} = \frac{R}{P} \quad (10)$$

The rationale for this assumption is that the sample fluxes, while not equal to the full components due to some unavoidable turbulent mixing

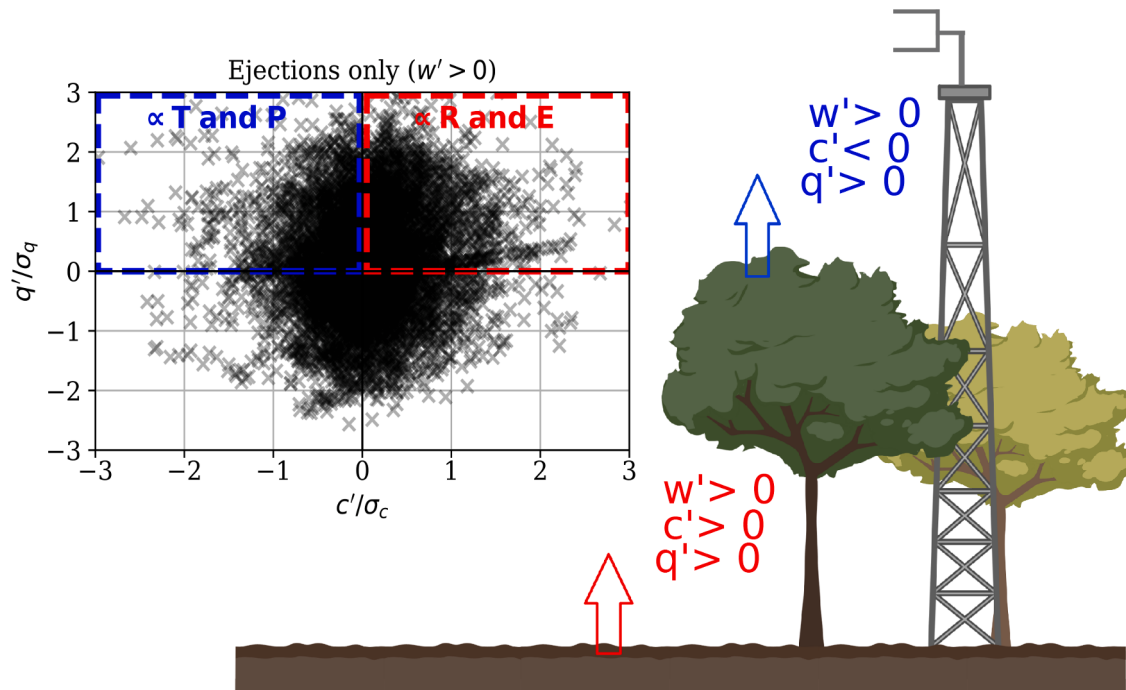


Fig. 1. Conceptual framework underlying the Conditional Eddy Covariance (CEC) partitioning method. The quadrant plot displays a 30-min time series measured over a grass site in Kenya. The quadrants used are conditioned on ejections; thus only points that obey $w' > 0$ are included in the figure.

and smearing of source/sink signatures and due to the ignored complex role of sweeps, remain good statistical surrogates for them. Thus, the ratio of the sample fluxes is now proposed as a measure of the ratio of the component fluxes. Combining these ratios with total fluxes, $ET = T + E$ and $F_c = P + R$ we obtain

$$E_{\text{CEC}} = \frac{ET}{1 + \frac{1}{r_{ET}}} \quad \text{and} \quad T_{\text{CEC}} = \frac{ET}{1 + r_{ET}}, \quad (11)$$

$$R_{\text{CEC}} = \frac{F_c}{1 + \frac{1}{r_{F_c}}} \quad \text{and} \quad P_{\text{CEC}} = \frac{F_c}{1 + r_{F_c}}. \quad (12)$$

In this expression, the total fluxes are computed using all data from all octants (conventional EC) and should also include any additional post-processing corrections that are not applicable to instantaneous fluctuations. For instance, while q' and c' should already be corrected for density fluctuations (Dettò and Katul, 2007), only ET and F_c would be affected by frequency loss corrections. Thus, the total fluxes used in Eqs. 11 and 12 should already take any additional corrections for the mean statistics into account. The same applies to the MREA and FVS methods.

To ensure that fluxes are computed with a representative number of points, we apply the constraint that together, the first and second octants ($\sum I_E + \sum I_T$) must contain at least 20% of the data points. In addition, if any of the two octants contains less than 5% of points, all fluxes are attributed to the other component; for instance, if the indicator functions in Eq. (9b) register at least 20% of points, and O1 and O2 independently have more than 5% of points, the partitioning method is implemented as described. On the other hand, if both octants add to 20%, but O1 (O2) contributes to less than 5% of points, all fluxes are attributed to plant (ground) components. For consistency across methods, the same constraint is applied to MREA despite the fact that it only uses direct observations from the first octant.

The only mathematical constraint on this method occurs when $R \approx -P$ (i.e., when $r_{F_c} \approx -1$), which is near a singularity of the equations for P and R . In this limit, two cases are possible: either both components are negligible (less likely to occur in vegetated ecosystems), or P and R nearly balance. The same constraint is also applicable for the FVS method, given that it computes the ratios $R_{\text{FVS}}/P_{\text{FVS}}$ from equation (3b),

and later computes the components using the same expressions as shown in equation (12). Thus, the results for F_c components for both CEC and FVS must be scrutinized near this singularity. This constraint on F_c does not pose problems for the results of ET components, which are not subject to similar mathematical constraint since both component fluxes are directed upward and thus have the same sign. The mathematical singularity when $r_{ET} \approx 0$ for the CEC method, which might happen when there are few points in the first octant, is thus handled by assuming that all ET fluxes originate from canopy transpiration.

3. Description of sites and data processing

Four datasets over different ecosystems were selected to evaluate the performance of the three partitioning techniques. The first site — an irrigated grass field in Central Kenya — contains independent estimates of both transpiration and evaporation obtained by leaf-level measurements and isotopic techniques during a controlled experiment (Good et al., 2014). Despite the associated uncertainties of these approaches and additional uncertainty arising from upscaling to the footprint of the EC method, they can still offer an independent means of evaluation. The second site is a mature Ponderosa (MP) pine forest in Oregon that contains independent estimates of soil respiration measured by chambers. The same dataset — with data sampled below, mid, and above canopy — was previously used by Thomas et al. (2008) to evaluate the MREA method. The other two sites are a vineyard in California (Knipper et al., 2019) and a pine forest in the state of Washington. The latter site is located at the Wind River Experimental forest and is referred to as WRE forest here. These two sites do not have independent estimates of any of the components. Nonetheless, they have yearlong data allowing us to compare the performance of all three methods across different seasons (and foliage amounts) at these two different ecosystems. A description of the sites and their data is given below and also summarized in Table 1.

3.1. Sites description

The grass site is located at the Mpala Research Center in central Kenya (0.3229°N, 36.9028°E) (a picture of the site is shown in Fig. S1 in

Table 1

Summary of sites and eddy-covariance (EC) measurements used in the analyses. Shown are leaf-area index (LAI), mean canopy height (h), EC measurement height (z), and EC sampling frequency. The MP forest stands for mature Ponderosa forest, and WRE forest stands for Wind River Experimental forest.

Site	Coordinates	Period	LAI ($\text{m}^2 \text{ m}^{-2}$)	h (m)	z (m)	Freq. (Hz)
Grass field Central Kenya	0.3229°N–36.9028°E	Feb 6, 2011–Feb 21, 2011	0.1	0.05	0.40	10
MP forest Oregon, USA	44.425°N–121.557°W	June 16, 2006–July 16, 2006	2.8	15	33.5, 10, 4	20
Vineyard California, USA	36.8492°N–120.1760°W	May, 2018–March, 2019	3.7	2–2.5	4	20
WRE forest Washington, USA	45.8205°N–121.9519°W	July, 2018–May, 2019	1.4	74	50	20

the supplementary material). The experiment took place between the 6th and the 21st of February 2011, the middle of the dry season. A circular plot of 530 m² was manually watered for 3 days starting on the 8th (the site had not received rainfall for 49 days prior the experiment). One additional rainfall event was registered on February 16. Following the irrigation of the soil, measurements of isotopic composition of water in the soil, atmosphere and leaves were obtained (for details of the methods and sensors see Good et al. (2014)). Green leaf coverage (GLC) was estimated by surveying two 26-m line transects, and was then related to LAI as $\text{LAI} = -\ln(1 - \text{GLC})$ (Nilson, 1971). Following this procedure, the maximum LAI observed throughout the experiment was 0.1 m² m⁻².

At the site, transpiration was estimated by leaf-level measurements using a chamber-based hand-held photosynthesis system (model Li-6400XT, LiCor Biosciences¹, Lincoln, NE, USA), with measurements of three to five leaves at approximately hourly intervals between 10 am and 5 pm local time each day. Transpiration rates per unit leaf area were later scaled by measurements of LAI based on transect surveys to estimate transpiration values per square meter within the watered area. Moreover, an EC system consisting of a three-dimensional sonic anemometer (model CSAT-3, Campbell Scientific, Logan UT) and an infrared gas analyzer (model Li-7500, LiCor Biosciences, Lincoln NB) was setup at 40 cm above the ground. This height is ≈ 4 times the sonic path length, and as such the EC signal mainly resolves the largest eddies contributing to the fluxes. However, since the measurements are mainly during the daytime, the contribution of the unresolved eddies is not expected to be large in the convective boundary layer (we will discuss possible implications in the results section).

The second site is a mature ponderosa pine forest (MP forest) located east of the Cascades Mountains crest near Sisters, Oregon, USA (44.425°N, 121.557°W). With a mean tree height of 15 m, this forest has a mean tree density of 325 trees ha⁻¹ and a maximum LAI of 2.8 m² m⁻² (Irvine et al., 2008; Thomas et al., 2009). The understory canopy is sparse, with an LAI of approximately 0.2 m² m⁻², mainly composed of bitterbrush (*Purshia tridentata*) and Manzanita (*Arctostaphylos patula* Greene). The same dataset originally used by Thomas et al. (2008) to evaluate the MREA method is used here. Eddy-covariance measurements from three vertical levels are available: 33.5 m (above canopy), 10 m (mid canopy), and 4 m (below canopy). All levels were instrumented with the same sonic anemometer and infrared gas analyzers (CSAT-3 and Li-7500, respectively). In total, one month of data (June 16, 2006–July 16, 2006) is used. The site received 55 mm of rainfall in the two weeks before the start of record (between June 1st and June 16) and an additional 16 mm during the period of analysis. Concurrent to eddy-covariance data, automated chambers (Irvine and Law, 2002; Irvine et al., 2008) were used to measure soil respiration. In total, ten spatially distributed chambers of 0.21 m² each were used. Soil respiration was sampled every 60 min and all 10 chambers were spatially

averaged. To compare with EC estimates, hourly estimates were interpolated to half-hourly values.

Data over a vineyard, located 25 km west of Fresno (36.8492°N, 120.1760°W), California, were collected as part of the USDA-ARS grape remote sensing atmospheric profile and evapotranspiration experiment (GRAPEX) (Kustas et al., 01 Sep. 2018). Vines are 1.5 m apart and planted in parallel rows separated by a distance of 3.35 m (Knipper et al., 2019). The vineyard is divided into four sections of nearly identical areas, each equipped with an eddy-covariance tower in the southwest corner to maximize fetch within the block (Knipper et al., 2019). Given the similarities across the four blocks during most periods of the year, we report results for only one of them. The site is equipped with a variable rate drip irrigation system capable of applying specific amounts of irrigation on a 30 m × 30 m gridded basis (a schematic of the position of the vines, the tower and the irrigation lines is shown in Fig. 1 of Knipper et al. (2019)). However, as a controlled stress experiment, the site was not irrigated between June 14, 2018 and July 23, 2018. The EC flux measurements were obtained by a Campbell Scientific, Inc. (Logan, UT) IRGASON H₂O/CO₂ sensor, which integrates the open path gas analyzer and the sonic anemometer. The EC system was mounted 4 m above ground level, while the mean canopy level varied between 2.0 and 2.5 m.

We used data measured over the vineyard from May 2018 to March 2019. To facilitate the assessment of the results, we separate the data into three ranges that characterize the vegetated conditions at the site: green foliage, transition, and bare soil (pictures of the site taken in each period can be seen in the supplementary material). Green foliage includes the period between May and September (late spring to early fall). In this phase, vines reach their maximum leaf area index (LAI nearly 3.7 m² m⁻², measured through ground sampling (White et al., 2018)) and are photosynthetically active; the interrows, on the other hand, are either bare soil or senescent cover crop. In addition, the green foliage season is a hot and dry period, drip irrigation being the only source of water. As a consequence, the volumetric water content (VWC) is low in the interrows, being larger near the points of irrigation under the plant canopy (see Fig. 2a; pictures of the drip irrigation system are available in the supplementary material). By mid-fall, leaves undergo senescence and there is a cover crop planted in the interrows (LAI nearly 1.4 m² m⁻²). This transition period (here defined from October to January) is wet because of the rainfall events, increasing soil moisture. It is also characterized by lower temperatures and vapor pressure deficit (VPD). February to late March is a period of bare soil, with complete absence of vegetation.

The last site is located at the Wind River Experimental Forest (45.8205°N, 121.9519°W), 60 km northeast of Vancouver, WA. This site is part of the National Ecological Observatory Network (NEON). While best known for its old-growth Douglas fir (*Pseudotsuga menziesii*) and western hemlock (*Tsuga heterophylla*) stands, the forest is a mosaic of tree ages due to management practices and wildfire history (National Ecological Observatory Network, 2020b). It is dominated by an evergreen forest with a mean canopy height of 50 m (phenocam images of the site (National Ecological Observatory Network, 2021c) are shown in the supplementary material). The leaf area index, estimated from flight line images taken in July 2019, is on average 1.4 m² m⁻² (National Ecological Observatory Network, 2021e). At the site, the EC system was

¹ The use of trade, firm, or corporation names in this article is for the information and convenience of the reader. Such use does not constitute official endorsement or approval by the US Department of Agriculture or the Agricultural Research Service of any product or service to the exclusion of others that may be suitable.

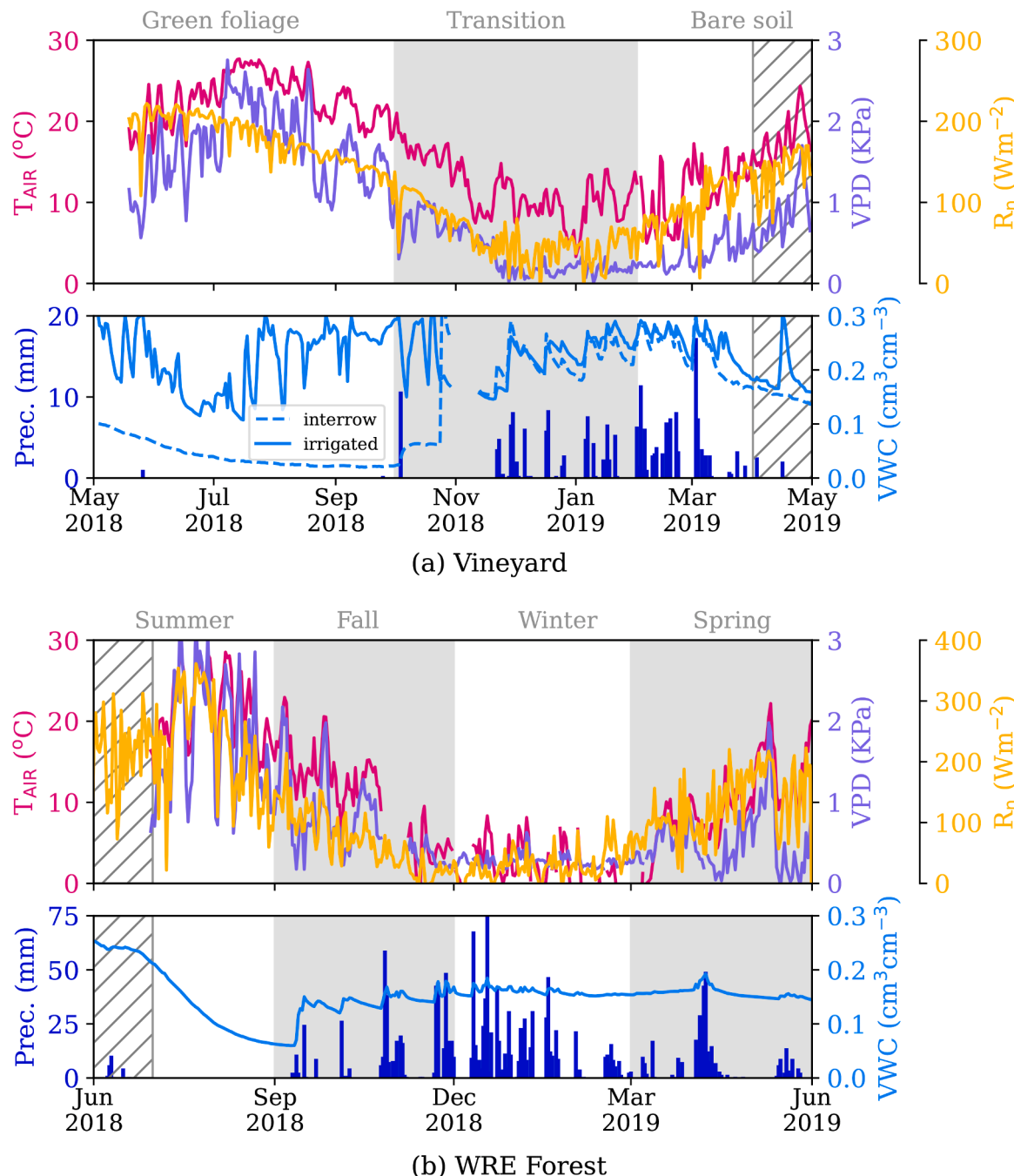


Fig. 2. Summary of meteorology and soil moisture at (a) the vineyard in California and (b) the WRE forest in Washington. Shown are daily averages of air temperature (T_{AIR}), net radiation (R_n), vapor pressure deficit (VPD), and soil volume water content (VWC). Daily accumulated precipitation is also depicted. The VWC was measured 5 cm below the surface at the vineyard and 6 cm below the surface at the forest. For the vineyard site, we show VWC measured in the middle of the interrow (dashed line) and measured 37 cm from one of the drip irrigation points (continuous line). Hatched areas indicate periods when data were not available (forest) or not included (vineyard) in the partitioning analysis.

placed at 74 m above the ground and includes an enclosed gas analyzer (model Li-7200, LiCor Inc., Lincoln, NB) and a three-dimensional sonic anemometer (model CSAT-3, Campbell Scientific Inc., Logan, UT) acquiring data at 20 Hz. The raw data were downloaded from NEON EC Level 0 prime (L0) product (National Ecological Observatory Network, 2020a). Precipitation (National Ecological Observatory Network, 2021a), radiation (National Ecological Observatory Network, 2021b) and soil water content (National Ecological Observatory Network, 2021d) were also downloaded from NEON Data Products (National Ecological Observatory Network, 2021f). Here, we used nearly a year of data from July 2018 to May of 2019, which we grouped into four

seasons, with summer including only July and August of 2018. The summer was very dry and did not register any rainfall event, but as shown in Fig. 2b, the volumetric water content was high at the beginning of that season, declining to nearly $0.06 \text{ cm}^3 \text{ cm}^{-3}$ in early fall. With the increase in rainfall events, VWC increases to an average $\sim 0.16 \text{ cm}^3 \text{ cm}^{-3}$ from fall to spring.

To summarize, we are contrasting four ecosystems with different canopy structures and leaf area indices. Two of them (grass site and MP forest) have independent estimates of ET or F_c components available. The other two sites (vineyard and WRE forest) do not have independent estimates, but can be analyzed across different seasons to investigate the

annual evolution of the partitioned fluxes. The grass site has the lowest vegetation height of about 5 cm, with a maximum LAI of $0.1 \text{ m}^2 \text{ m}^{-2}$; the EC system is placed at 8 times the grass height. The vineyard has a peak LAI of $3.7 \text{ m}^2 \text{ m}^{-2}$ during summer, which decreases as the crop matures and reaches zero in the bare soil phase. The EC system is placed at 4 m, about 2 times the typical vines height (between 2 and 2.5 m). The WRE forest, on the other hand, has a lower average LAI of $1.4 \text{ m}^2 \text{ m}^{-2}$, but a higher canopy (≈ 50 m); its EC system is at about 1.5 times that elevation. The MP forest, with an LAI of about $2.8 \text{ m}^2 \text{ m}^{-2}$, has three measurement levels where z/h is in the range 0.26–2.2. The differences in LAI, canopy height and EC system height offer a range of conditions that challenge the applicability of the three methods in different ways, as we will discuss.

3.2. Data processing

Post-processing controls were performed to ensure that only high quality raw time series were retained. Values outside realistic bounds were deleted (for instance, negative concentrations), and outliers were detected with a despiking routine (Zahn et al., 2016) and then removed. In addition, when available, the diagnostic flag of the sonic anemometer and the signal strength (the replacement of the Automatic Gain Control (AGC) indicator in LiCor systems) for CO_2 or H_2O were used. In this case, CO_2 or H_2O measurements with a signal strength $< 70\%$ (below which the windows of the analyzer should be cleaned) were deleted. Small gaps (up to four consecutive points) were filled by linear interpolation. Finally, we only retained periods where at least 90% of the instantaneous data points were available. For the NEON forest site with an enclosed-path system, a correction for the velocity-concentration time lag was applied by performing a cross correlation analysis (Metzger et al., 2018; Rebmann et al., 2012).

Double coordinate rotation was performed to align the mean velocity with the streamwise direction, and linear detrending of the mean was applied before computing fluctuations. Strongly non-stationary periods were filtered out based on the test proposed by Foken (2017, p. 175); periods were removed whenever the non-stationarity statistic for $w'c'$ or $w'q'$ (instantaneous products) was above 25%. Pre-hoc density fluctuations of carbon and water vapor measured by the open-gas analyzers (LI-7500 and IRGASON) were corrected to take into account the effect of external fluctuations (Detto and Katul, 2007) (equivalent to the post-hoc Webb-Pearman-Leuning correction (Webb et al., 1980), but correcting instantaneous values). To avoid distortion in the flow field caused by the tower, we also excluded periods when the mean wind direction is from behind the tower. All fluxes were computed over 30-min periods.

The water-use efficiency, which is required by the FVS method, was computed using Eq. (5). The mean concentrations near the canopy, \bar{c}_c and \bar{q}_c , were computed based on the gradient function from the Monin-Obukhov similarity theory. However, these functions were not applied to data sampled below the canopy at the MP forest. Instead, we assumed that the same WUE computed on a half-hourly basis above the canopy was also valid at the levels below the canopy.

The intercellular CO_2 concentration (\bar{c}_s) is the most challenging variable and is parameterized with different formulations outlined in previous implementations of FVS (Skaggs et al., 2018). It can be assumed that \bar{c}_s is a constant value, that its ratio to near canopy concentration \bar{c}_s/\bar{c}_c is constant, or that \bar{c}_s/\bar{c}_c is a function (linear or to the 1/2 power) of the atmospheric vapor pressure deficit (a summary of formulations for \bar{c}_s is given in Katul et al. (2000)). More recently, Scanlon et al. (2019) proposed an optimization model for WUE that circumvents the parameterization of \bar{c}_s . This model, which maximizes carbon assimilation while minimizing water losses, is computed using only EC data. In our implementation of FVS, all five models (constant \bar{c}_s , constant ratio, linear and 1/2 power function of VPD, and optimization model) were used (as described in Appendix A). None of these models takes plant stress into account (i.e., plant response to conditions of

limiting water or high VPD). The results presented here are the ensemble average of different estimates of the four flux components, computed when at least one parameterization of \bar{c}_s resulted in valid solutions of the FVS partitioning. For example, the component transpiration shown in our results for this method represents the ensemble average of up to five T_{FVS} values (one for each parameterization of \bar{c}_s), depending on which parameterizations resulted in valid estimates.

4. Results and discussion

4.1. Convergence to physical solutions

In this section we report the frequency at which all three methods successfully found physically plausible solutions given the constraints imposed on their formulation, as detailed in the previous sections. Note that this analysis only indicates how often solutions are available for each method, but cannot inform on how accurate these solutions are. Thus, a method that results in more solutions is not necessarily a more accurate approach.

Because all three methods result in more variability in time for F_c than ET components, we also imposed the following additional conditions to admit the calculated carbon dioxide fluxes (for all three methods): R and $|P| < 2.5 \text{ mg CO}_2 \text{ m}^{-2} \text{ s}^{-1}$ over the vineyard and WRE forest, R and $|P| < 1.0 \text{ mg CO}_2 \text{ m}^{-2} \text{ s}^{-1}$ over the MP forest, and R and $|P| < 0.5 \text{ mg CO}_2 \text{ m}^{-2} \text{ s}^{-1}$ over the grass field. These values were selected to be plausible upper limits based on results from half-hour periods and to ensure removal of outliers. A summary of the main causes of discarded solutions for each method is shown in Table A1 and Table A2.

In Fig. 3, we show the percentage of periods when an admissible solution was found by each of the three methods over the MP forest (3 a), vineyard in California (3 b) and WRE forest in Washington (3 c). It only includes cases when all four components were successfully found; for instance, if CEC did not find a valid solution for R and P since they nearly balance each other as previously explained, we do not count this period even though E and T were successfully computed. In addition, we keep results obtained by FVS during nighttime periods (shaded area in the figures), although in principle the method is not appropriate for this time of the day because of the absence of photosynthesis and transpiration (and an undefined WUE). In this case, we still compute the water-use efficiency using the same equations we apply during the day, but the results may be unphysical. Nonetheless, FVS is not applied over the vineyard during the bare soil period because of the absence of leaves in this period (the computation of WUE involves defining the leaf temperature).

The large fraction of solutions found between hours 8 and 16 indicates that all methods perform better during daytime when fluxes are stronger. Among the methods, FVS has the lowest rate of convergence, which is mainly caused by the failure to satisfy Eq. (4). For instance, the method did not converge most of the time below the canopy at the MP site. MREA, on the other hand, has a high rate of convergence during daytime, but it drops during night-time hours. In most of these periods, the constraint $E \leq ET$ (also $R \leq F_c$) was not satisfied. Visual inspection of these results confirmed that in such cases E was significantly greater than ET and not only an artifact of round-off errors. Regarding CEC, it found acceptable solutions more frequently, particularly during night-time when it was able to attribute the total fluxes ET and F_c to E and R components, respectively, most of the time.

The lowest rate of convergence for CEC happened at the mid canopy level of the MP forest. The main cause of flagged nonphysical solutions was the low F_c , often $\lesssim 0.2 \text{ mg CO}_2 \text{ m}^{-2} \text{ s}^{-1}$ during the month. During the day, such small fluxes were usually the result of the near balance between P and R , which might lead to a singularity in Eq. (12) if $r_{F_c} \approx -1$. Thus, for this dataset we neglect solutions for F_c components whenever $-1.2 < r_{F_c} < -0.8$. Note that ET components are not affected by this convergence issue and are not neglected: even if the two carbon fluxes cancel out to result in a small F_c , their correlation with the water

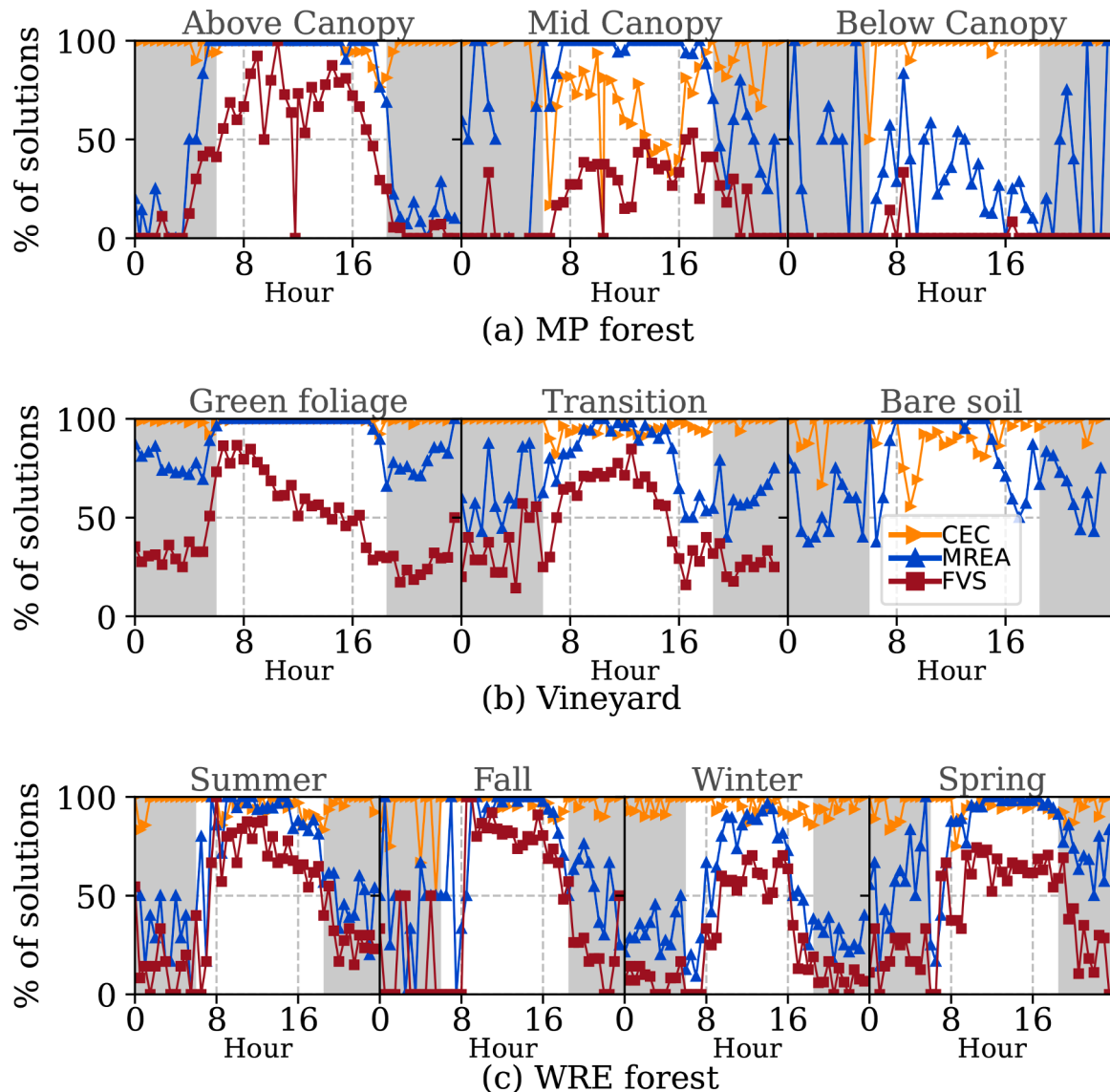


Fig. 3. Percentage of available time blocks for which an admissible solution was found over the MP forest (a), the vineyard (b), and the WRE forest (c). For the MP forest, convergence for a month of data (16 June–16 July, 2006) at three canopy levels is shown. Data obtained at the vineyard were split into three categories that reflect different stages of the site: green foliage (May to September of 2018), transition (October of 2018 to January of 2019), and bare soil (February and March of 2019). Data for the WRE forest were split into the four seasons, with summer starting in July of 2018. The FVS was only applied when leaves were present, which excluded months of bare soil in the vineyard. Shaded area represents nighttime periods. (For interpretation of the references to colour in this figure legend, the reader is referred to the web version of this article.)

fluxes needed to partition ET is not affected. The same r_{F_c} constraint was applied to the carbon dioxide flux components computed by the FVS method. Nonetheless, the main cause for invalid solutions for the FVS method across all sites was the violation of the condition in Eq. (4).

For the Kenya grass site (not shown in the figure), in total, two weeks of data — sampled only during daytime — were available. For this site, CEC converged to physically valid solutions 95% of the time. The main cause of failure to its convergence in the remaining 5% of blocks happened halfway through the experiment, when the increase in plant photosynthesis reduced the net carbon dioxide flux to $\approx 0.1 \text{ mg CO}_2 \text{ m}^{-2} \text{ s}^{-1}$. Under these conditions, P and R were nearly balancing, leading to the previously-discussed singularity in the equations. Similar to what was noted at the mid canopy level of the MP forest, most of the noisy periods were observed when $-1.2 < r_{F_c} < -0.8$; thus, we neglected R_{CEC} and P_{CEC} computed over the grass site when r_{F_c} was in this range.

Independent of the parameterization used to compute water-use efficiency, the FVS method did not find solutions over the grass site in Kenya. In most of the half-hour time windows of the two-week dataset,

the mathematical constraints that ensure physically realistic fluxes (equation (4)) were not satisfied. The removal of low frequencies — as suggested by Scanlon and Kustas (2010); Scanlon and Sahu (2008) — using a high-pass Gaussian filter did not increase the convergence of the method. In Section 4.2, when comparing the partitioning approaches over this site, we included the transpiration and evaporation computed by FVS as reported in Good et al. (2014). Good et al. (2014)'s results were obtained with a previous version of the model that consisted of numerically finding solutions and did not include the constraints in Eq. (4); in addition, the authors implemented wavelet filtering to continuously remove low frequencies of the time series and search for a valid solution, which increases the rate of convergence of the approach (verified through analyses done for the present study).

Over the grass field, the MREA method found valid physical solutions nearly 30% of the time. Invalid solutions were flagged for $T_{\text{MREA}} < 0$ or $P_{\text{MREA}} > 0$ (at least one condition had to apply). These periods were identified to happen more often during periods when the correlation coefficient between water vapor and carbon dioxide densities was

strongly positive (similar to FVS). In other words, MREA is more successful in converging to physically valid solutions when plant components dominate, i.e., when $\rho_{c,q} < 0$. This behavior for both MREA and FVS can be seen more clearly below the canopy at the forest in Oregon (Fig. 3). As shown in the figure, at this site these methods found solutions more often above and in the middle of canopy, where $\rho_{c,q} < 0$ is to be expected. Below canopy, on the other hand, non-stomatal components dominate and the methods found solutions less frequently.

In contrast to FVS and MREA, CEC is less affected by the correlation between the scalars. This result indicates that CEC can be applied to a wider range of $\rho_{c,q}$ conditions resulting in less gaps, although it does not

guarantee that the solutions are accurate. Nonetheless, as shown both above the grass site and in the middle of the canopy of the MP forest, its convergence rate drops when a small F_c is observed as a result of near balance between R and P .

4.2. Evaluation of partitioned transpiration against leaf-level measurements

A comparison of all partitioning estimates available for the grass site in Kenya (three EC methods, isotope method, and leaf-level measurements) is shown in Fig. 4. Daily averages and standard error based on the

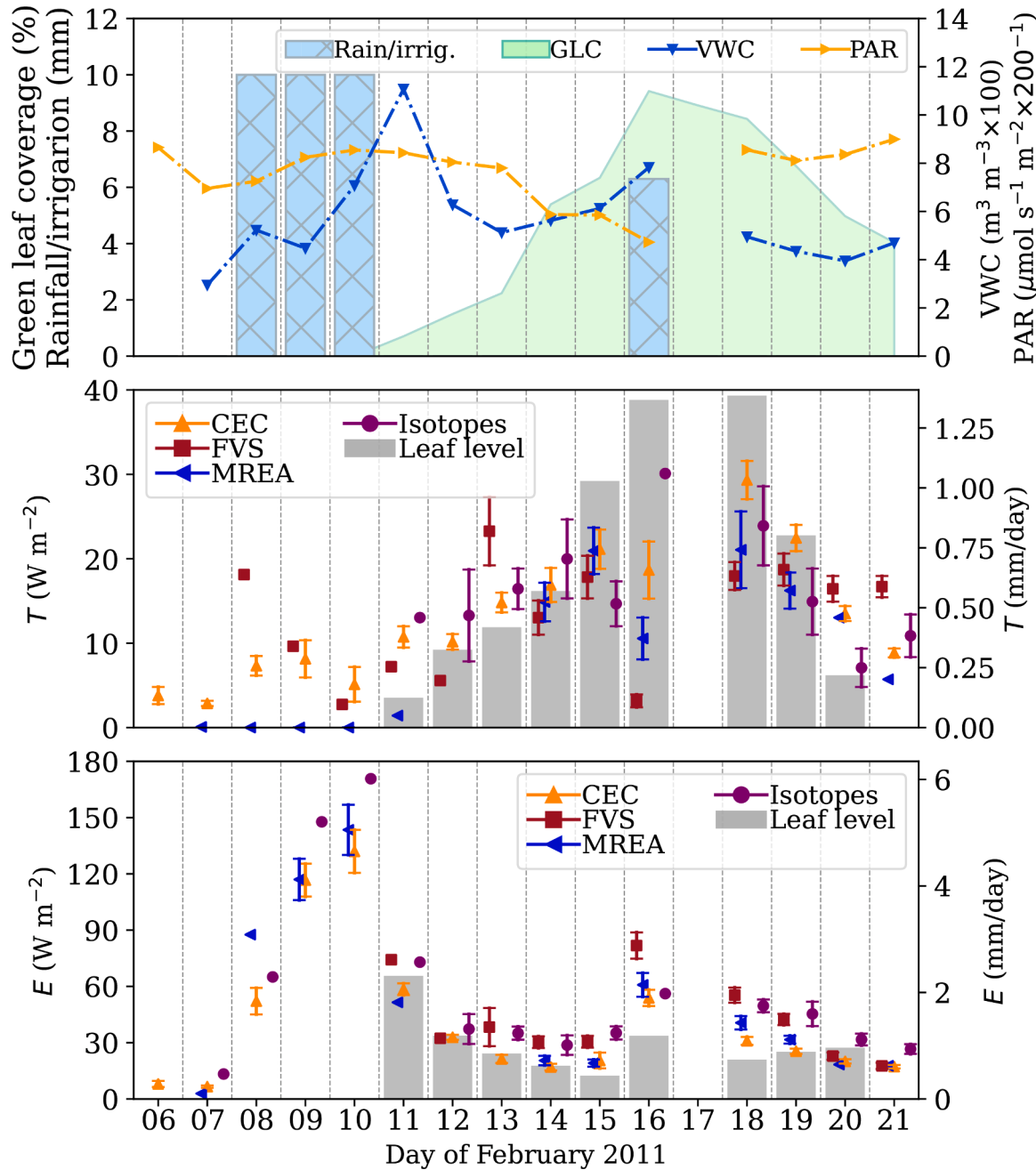


Fig. 4. Top panel shows green leaf coverage (GLC), wetting of the region by irrigation or rainfall along with the soil volumetric water content (VWC), and photosynthetically active radiation (PAR). The daily averaged transpiration (middle panel) and evaporation (bottom panel) are also depicted using various methods (right axis shows values in mm/day). For the partitioning obtained using CEC, FVS, MREA, and isotopes, symbols represent the average and bars denote one standard error from the mean (calculated for the EC-based methods from 30-min period values relative to the daily mean, and only when at least three periods or observations were available for a given method). Evaporation from leaf-level measurements is computed as the difference between average ET (from EC measurements) and average T_{leaf} . FVS results are taken as reported in Good et al. (2014). (For interpretation of the references to colour in this figure legend, the reader is referred to the web version of this article.)

30-min fluxes (when at least three observations during the day were available) are shown, with the exception of leaf-level transpiration for which only the average is shown (grey bars). Note that each method may have found valid solutions for different time blocks between 9 am and 5 pm; therefore, average transpiration and evaporation may not add to the total ET for all methods. Furthermore, the FVS results are those reported in Good et al. (2014) as our implementation of the method (with constraints that were suggested more recently by the developer, as discussed above) did not converge to valid solutions.

Prior to the start of the experiment, the grass field was devoid of any green vegetation as indicated by the green leaf coverage in Fig. 4 (top plot). After three days of consecutive irrigation, green leaf coverage increases and reaches its peak on day 16. As expected, this photosynthetically active period leads to the increase in transpiration inside the delimited plot as measured by leaf-level chambers. As shown by footprint analyses conducted by Good et al. (2014), the flux measured after irrigation represents mostly the irrigated area ($\approx 85\%$ of total ET), as opposed to nearly 57% when the field is dry.

The transpiration estimated by FVS, T_{FVS} , does not follow the trend found by leaf-level measurements over the observational period. It overestimates transpiration on day 8, prior to the increase in green area coverage, and again on day 13. Moreover, it shows weak variation between days 18 and 21, when all other methods capture a decrease in transpiration that resulted from the decrease in green leaf density. The MREA method also did not find solutions for all time intervals, where nearly half of the days have less than three data points available. Nonetheless, the trends and magnitudes of the daily averaged T_{MREA} on days 14 to 19 are close to the other estimates.

The transpiration computed by CEC, T_{CEC} , seems to follow the same trend as the green-leaf area coverage: it increases with green leaf coverage between days 11 and 15 and later decreases from days 18 to 21, when the field is getting drier and less green. On day 16, it shows a drop in transpiration (and increase in E_{CEC}), which, despite not matching leaf-level estimates, is consistent with a decline seen in photosynthetically active radiation during this cloudy day (bottom plot in Fig. 4). After day 17, E_{CEC} also decreases as the volumetric water content decreases. In addition, E_{CEC} dominates over T_{CEC} before and during irrigation (days 6 to 10). Overall, the ratio T_{CEC}/ET computed from the respective daily accumulated values varies from 0.04 on day 9 to 0.51 on day 15. However, the instantaneous value of T_{CEC}/ET (from half-hourly fluxes) is as high as 0.74 at 1:30 pm on day 15. Note that T_{CEC} was non-zero even before the irrigation ($T_{CEC}/ET < 0.3$); this signal is likely coming from outside the delimited area where the presence of sparse trees can be noted, which is corroborated by footprint analysis (Good et al., 2014).

Table 2 shows the root mean square error (RMSE), bias, and correlation coefficient (ρ) of transpiration found by CEC, FVS, and MREA versus transpiration estimated by leaf-level measurements (T_{LEAF}) and the stable isotopes method (T_{ISO}). CEC resulted in the smallest RMSE ($4.7\text{--}5.9\text{ W m}^{-2}$) and highest correlation coefficients (0.7–0.96); it also had the lowest bias when compared to leaf-level measurements. Despite many missing periods, the MREA also performed well in terms of correlation, in particular against the leaf-level estimates ($\rho = 0.86$). The FVS method, while having the smallest correlation coefficient ($\rho < 0.47$), resulted in the smallest biases against the isotopic method, and similar RMSEs to those of MREA ($\approx 6\text{ W m}^{-2}$ against the isotopic method and $\approx 10\text{ W m}^{-2}$ against leaf-level). Overall, both FVS and MREA found less solutions at this site, which was mainly dominated by soil flux components, resulting in positive $\rho_{c,g}$. Thus, such conditions seem not to be ideal for the applicability of both approaches.

The sub-daily variation in transpiration and evaporation, as well as respiration and photosynthesis, are shown in Fig. 5 (bottom panel). Because our implementation of FVS did not find solutions for this site, results from this method are not included. Comparing CEC and MREA, evaporation was greater than or equal to transpiration during most of

Table 2

Statistics of departure of transpiration found by the three partitioning methods from independent estimates obtained by leaf-level measurements (T_{LEAF}) and stable isotopes (T_{ISO}). Shown are the root mean square error (RMSE) in W m^{-2} , mean bias in W m^{-2} , and correlation coefficient (ρ). Rainy and cloudy day 16 was excluded from the computation of these statistics.

	T_{LEAF}			T_{ISO}		
	RMSE	Bias	ρ	RMSE	Bias	ρ
CEC	5.92	-0.09	0.96	4.72	-1.52	0.71
MREA	9.11	4.95	0.86	6.23	1.60	0.53
FVS	10.45	2.29	0.47	6.41	-0.28	0.18

the experiment. In addition, a diurnal cycle for both components is clearly distinguishable, with larger transpiration in the middle of the day when radiation, and consequently photosynthesis, are larger (with exception of day 16, which was a cloudy and rainy day).

Before irrigation, most of the F_c comprised of respiration according to CEC (Fig. 5, top panel). A small fraction of fluxes is attributed to photosynthesis (and transpiration), likely related to the contribution from outside the control area as discussed above. During the three days of irrigation, R_{CEC} decreases (as well as total F_c as observed by the EC system), while P_{CEC} is small and nearly constant. As the green leaf coverage increases, P_{CEC} increases, which is expected given its coupling to transpiration. On days 14 and 15, the magnitude of respiration gets closer to the magnitude of photosynthesis as the total F_c decreases; as a result, CEC did not compute valid estimates of both components when $F_c \lesssim 0.1\text{ mg CO}_2\text{ m}^{-2}\text{ s}^{-1}$, which resulted in large oscillations between negative/positive values in the estimates of R_{CEC} (and also P_{CEC}) and/or magnitudes at least two times higher than those found in the remaining periods of the same day. These values were removed and are not shown in the figure. Following day 18, R_{CEC} suggests soil respiration returned to the same magnitude that was observed in the first half of the experiment.

For days when MREA found a solution, the estimated T and E are similar in magnitude to those found by CEC. However, the same is not true for F_c components. MREA suggests negligible photosynthesis between days 14 and 19, when CEC indicates the largest P fluxes. While we do not have independent estimates of soil respiration to objectively compare these results, the presence of green vegetation indicates that photosynthesis should be at its maximum during these days. These results also illustrate the main difference between both approaches: CEC includes information from the second octant to infer the ratio between components used to compute the final component flux, potentially mitigating the effects of partial signal loss due to mixing of the air parcels, which affects both quadrants. MREA, on the other hand, computes respiration directly from the first quadrant. In this case, it might result in underestimated fluxes in case of partial mixing of the air parcels.

4.3. Evaluation of partitioned respiration against soil chamber measurements

We now assess the soil respiration component computed by the three methods against independent estimates obtained from chamber measurements (R_{CH}) at the MP forest. In addition, this comparison is performed below ($z/h=0.1$), mid ($z/h=0.67$), and above canopy ($z/h=2.3$). All results are shown in Fig. 6, where we plot half-hourly R estimated from the three methods versus R_{CH} . To reduce scatter — which is expected given the underlying differences between EC and chamber measurements — we plot the average and one standard deviation from the mean for evenly spaced bins. Furthermore, following Thomas et al. (2008), we only include daytime periods (8 am to 5 pm) and periods when $\rho_{c,g} \geq -0.5$. This excludes periods when the canopy fluxes are dominant and the ground signal is negligible.

The bin-averaged soil respiration (also comprising stem respiration) computed by the FVS method, R_{FVS} , resulted in the best agreement with

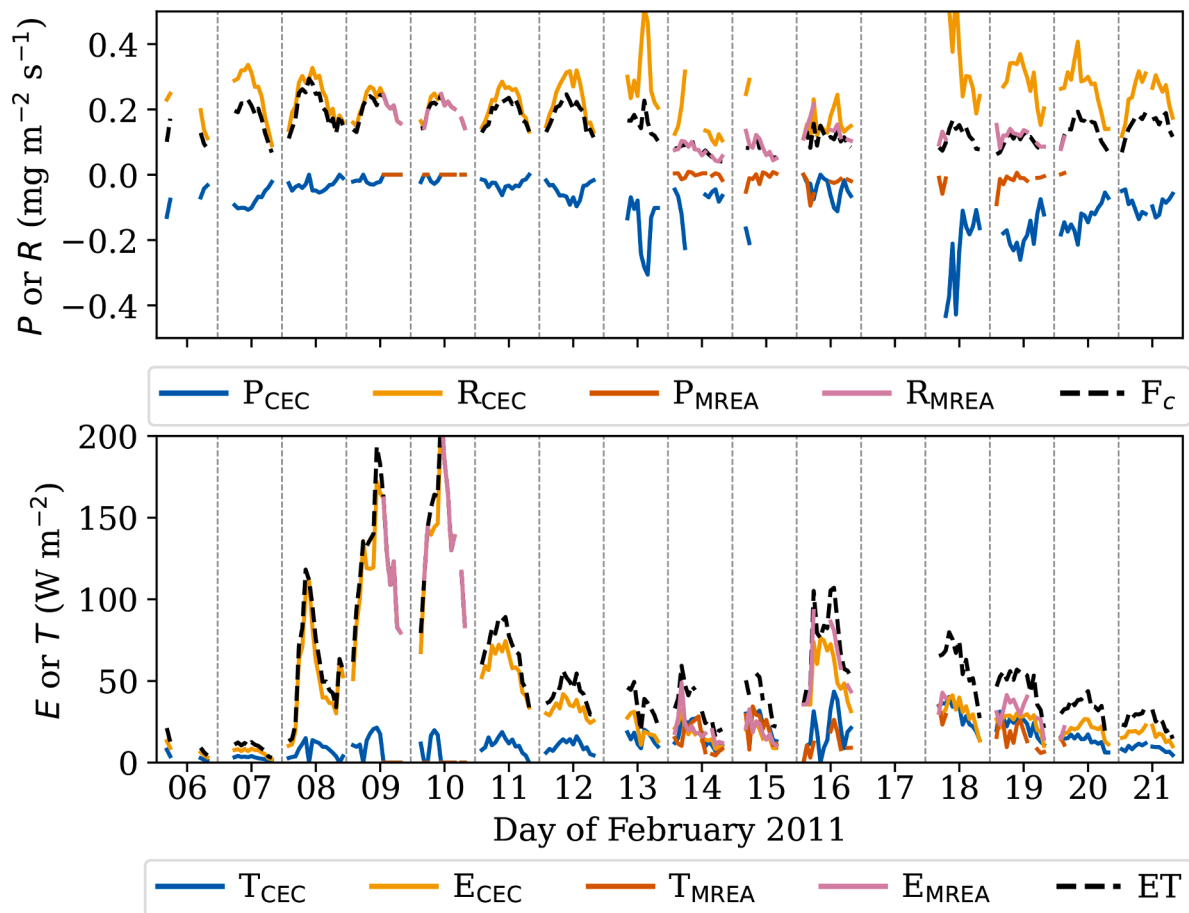


Fig. 5. Photosynthesis (P) or respiration (R , top panel) (both in $\text{mg CO}_2 \text{ m}^{-2} \text{ s}^{-1}$) and evaporation (E) or transpiration (T , bottom panel) computed using CEC and MREA for the grass site in Kenya. The dashed black lines represent total fluxes as observed by EC. Only fluxes between 9 am and 6 pm are shown. The MREA partitioning of water fluxes is not shown for many days because E exceeded total ET .

the independent estimates of soil respiration above the canopy. It found both the smallest RMSE and bias, 0.041 and $-0.004 \text{ mg CO}_2 \text{ m}^{-2} \text{ s}^{-1}$, respectively (Table 3; statistics were computed from bin averages). At this level, CEC and MREA performed similarly ($\text{RMSE} = 0.107\text{--}0.133 \text{ mg CO}_2 \text{ m}^{-2} \text{ s}^{-1}$, bias = $0.100\text{--}0.130 \text{ mg CO}_2 \text{ m}^{-2} \text{ s}^{-1}$), with both methods underestimating R_{CH} . The data for the individual periods, however, show more significant scatter, particularly for FVS.

The poor performance of CEC and MREA above the canopy might be a consequence of the large distance between the canopy and the EC sensors. As pointed out in previous studies (Klosterhalfen et al., 2019a; 2019b; Thomas et al., 2008), and further discussed in Section 4.5, the measurement height is one of the most important constraints for the applicability of similarity-based partitioning approaches. At $z/h = 2.2$ over this forest, air parcels carrying different scalar source and sink fingerprints are more likely to be mixed, scrambling the soil signature and resulting in large negative correlation coefficients between c' and q' , which adversely impacted both methods.

The performance of the three partitioning approaches diverges more at mid canopy. While CEC resulted in the smallest RMSE and bias (0.044 and $-0.006 \text{ mg CO}_2 \text{ m}^{-2} \text{ s}^{-1}$, respectively), it was also negatively correlated to R_{CH} (which is not the anticipated trend). From all investigated datasets, the mid canopy level at the MP forest was the most challenging for CEC in terms of CO_2 flux partitioning; the small F_c throughout the month resulted in noisier results for R_{CEC} than what was observed for FVS and MREA (or at other sites). Filtering periods when the ratio r_{RP} was in the range $-1.2 \leq r_{RP} \leq -0.8$ decreased — but did not remove — all possibly affected periods. Thus, in future implementations of CEC, we recommend careful analysis of CO_2 fluxes in this

limit when a small net carbon flux results from non-negligible but counteracting P and R . The best correlation with R_{CH} at mid canopy was found by the FVS method ($\rho = 0.81$), although it also overestimated the fluxes. MREA, on the other hand, underestimated R_{CH} , but correctly resulted in positive correlation (0.47).

The FVS method did not find solutions below the canopy. Note that we admitted the plausibility of below canopy P given the presence of a sparse ground vegetation. The fact that FVS did not converge might be indicative that P is negligible (non-negligible photosynthesis is required by the method). However, its performance may also have been impacted by the positive correlation between c' and q' below the canopy. As shown over the Kenya site, the method converges less often when soil fluxes dominate and $\rho_{c,q}$ is positive. In both cases, the mathematical constraints of Eq. (4) were not satisfied (more details in Table A1). The CEC and MREA methods performed better below the canopy. The respiration computed by both methods was highly correlated with R_{CH} ($\rho > 0.87$), with CEC showing slightly smaller errors ($\text{RMSE} = 0.024 \text{ mg CO}_2 \text{ m}^{-2} \text{ s}^{-1}$ and bias = $-0.001 \text{ mg CO}_2 \text{ m}^{-2} \text{ s}^{-1}$). Overall, these results below the canopy are encouraging and confirm that the proximity to sinks and sources improves the performance of CEC and MREA.

4.4. Seasonal and diurnal variation of flux components

In this section, we investigate the partitioning results across seasons over two contrasting ecosystems: a vineyard in California and a forest in Washington (WRE forest). As a point of reference, we present the average diurnal cycle of all four partitioning components; we also group periods with similar characteristics at the vineyard (green foliage,

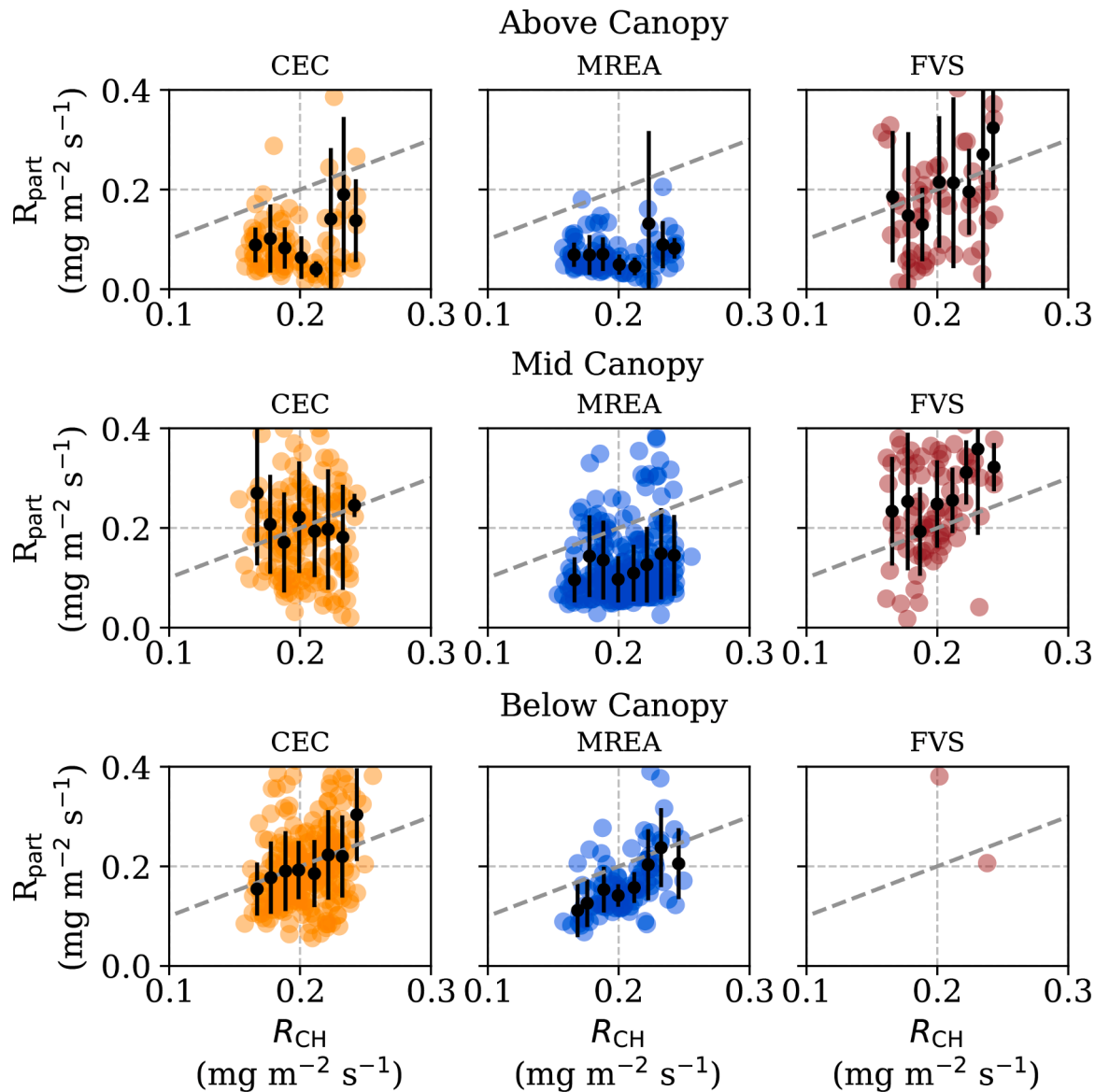


Fig. 6. Comparison of soil respiration (in $\text{mg CO}_2 \text{ m}^{-2} \text{ s}^{-1}$) estimated by the three partitioning methods (y-axis) versus soil respiration estimated by chamber measurements (R_{CH} , x-axis) at the MP forest. The variable R_{part} represents R_{CEC} (first column), R_{MREA} (second column), and R_{FVS} (third column). Results above canopy ($z/h = 2.2$, first row), mid canopy ($z/h = 0.67$, second row), and below canopy ($z/h = 0.25$, third row) are shown. Mean value for nine evenly spaced bins are shown in black, where the bars represent one standard deviation from the mean.

transition, and bare soil) and the four seasons at the forest. Averaged diel cycles over each month are included in the supplementary material. As detailed in the methods section, for FVS we plot the ensemble average for each component based on all parameterizations of WUE that resulted in solutions. To illustrate the variability across different options, we plot in Appendix Fig. B1 the diel cycle for all flux components as found by each WUE model for a selected period over the Vineyard and the WRE forest. In the most extreme cases, differences of more than 100% were seen across models.

Table 3

Error statistics of R estimated by the three (bin-averaged) partitioning methods against independent estimates of soil respiration obtained by chambers. Values for all three levels are shown. The statistics were obtained from the averaged bins shown in Fig. 6. RMSE and bias are given in $\text{mg CO}_2 \text{ m}^{-2} \text{ s}^{-1}$.

Above Canopy			Mid Canopy			Below Canopy			
	RMSE	Bias		RMSE	Bias		RMSE	Bias	ρ
CEC	0.107	0.100	0.55	0.044	- 0.006	- 0.23	0.024	- 0.001	0.87
MREA	0.133	0.130	0.40	0.083	0.080	0.47	0.044	0.039	0.91
FVS	0.041	- 0.004	0.81	0.075	- 0.067	0.81	—	—	—

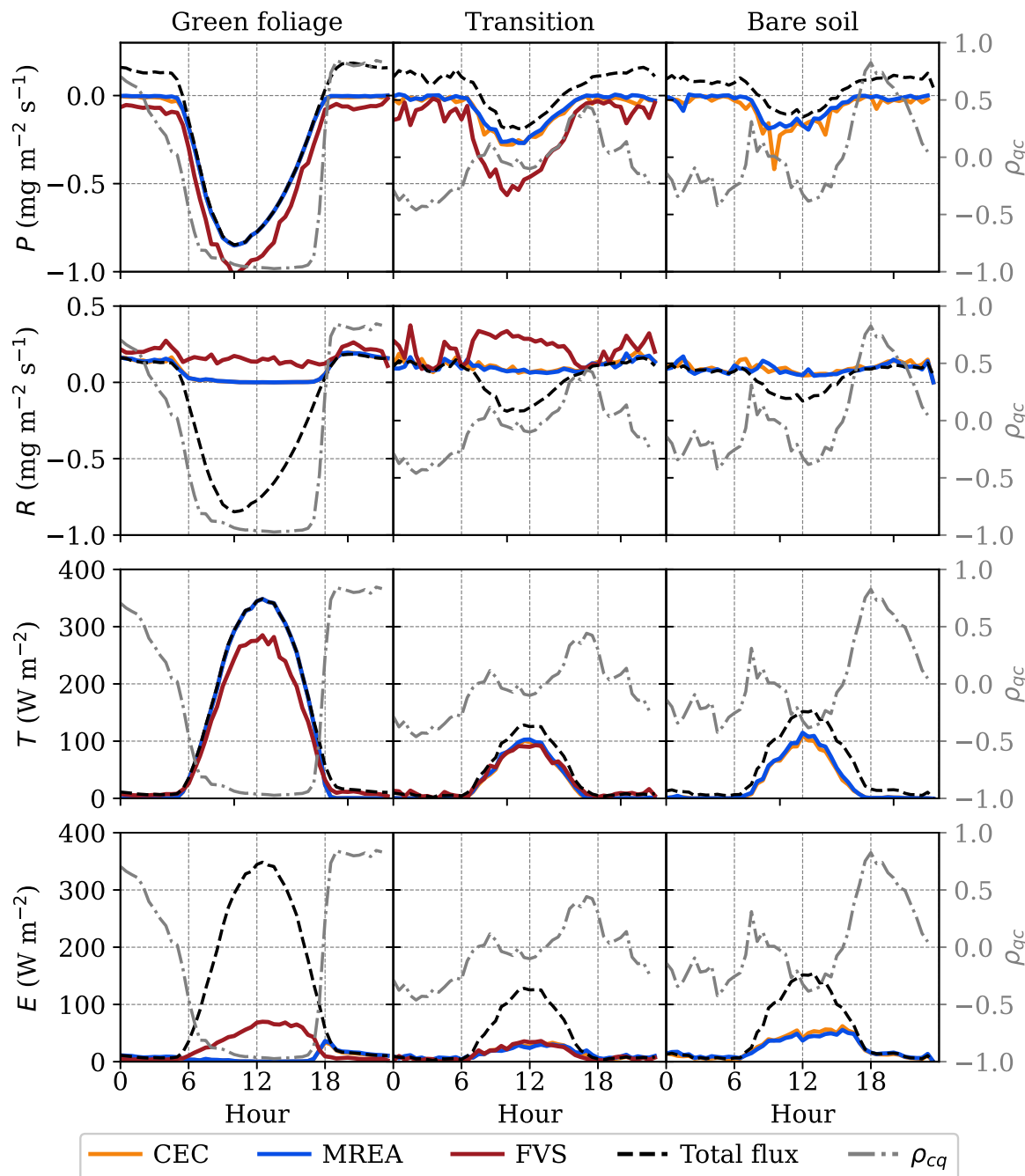


Fig. 7. Comparison of partitioning components obtained over the vineyard. The average diel cycle during each period is depicted, with dashed black lines representing the total EC fluxes of water and carbon dioxide computed using all available data (i.e., it does not exclude data when solutions were not found by one or more of the methods). The category green foliage includes the months of May to September 2018, transition includes October 2018 to January 2019, and bare soil includes February and March 2019. The CEC and MREA results were the same during the green foliage period, causing the yellow and blue lines to overlap. The FVS method was not applied during bare soil conditions because it assumes the presence of leaves. (For interpretation of the references to colour in this figure legend, the reader is referred to the web version of this article.)

that the MREA results were more sensitive to the newly imposed constraints of only accepting periods when $E < ET$ and $\sum I_E + \sum I_T \geq 20\%$. Without these constraints, MREA tended to overestimate nighttime respiration in all investigated sites, which resulted in non-negligible photosynthesis during nighttime hours. Thus, we recommend the adoption of these new constraints in future implementations of the MREA method.

Both R_{CEC} and R_{MREA} are negligible during the day, indicating no soil respiration. As a reminder, the photosynthesis computed here is the net photosynthesis, which is the difference between carbon assimilation and

leaf respiration. Therefore, if soil respiration is indeed negligible during the day when compared to above-ground respiration (as both methods indicate, though we cannot quantify the accuracy of this result), the nighttime respiration would be mainly from leaves (which we cannot compute separately during the day). While zero soil respiration might be a contradictory result given its positive relation to temperature (Reichstein et al., 2005), a dramatic decrease in soil CO₂ fluxes is to be expected during very dry periods (Xu et al., 2004). Thus, the low soil moisture (Fig. 2a) in the interrows during this phase (from 0.10 cm³ cm⁻³ in early May to less than 0.03 cm³ cm⁻³ in late September) would

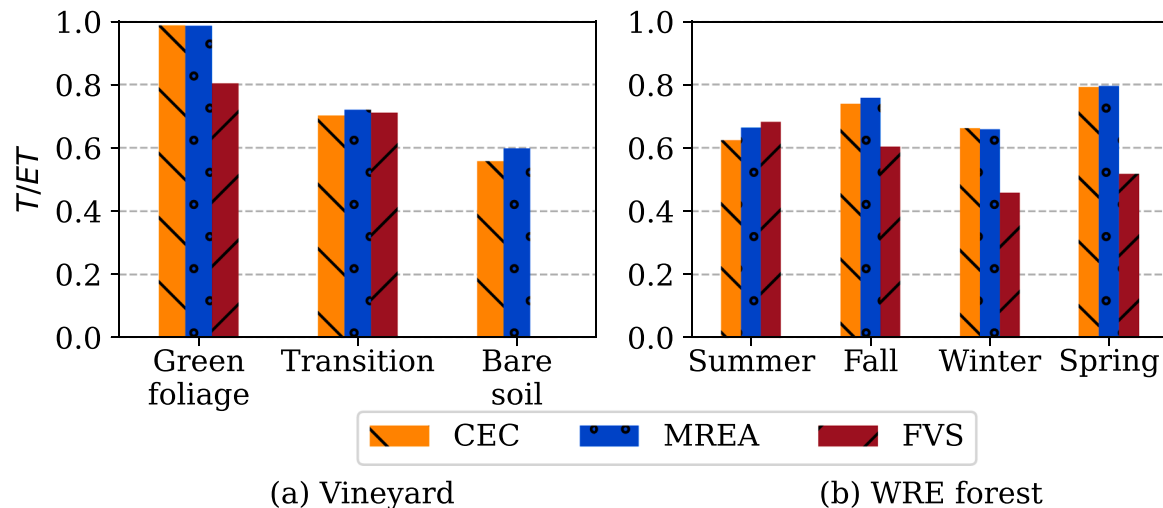


Fig. 8. Ratio of transpiration to evapotranspiration found by all three partitioning methods over (a) the vineyard and (b) WRE forest. Values were computed based on the accumulated T and ET over the average diel cycles shown in Fig. 7 and 9. However, for each method, we only used ET data when the respective method found a valid solution for T . In addition, only values between 7 am and 6 pm were used.

likely result in weaker soil fluxes (both respiration and evaporation) compared to the canopy. In addition, the only irrigated patches during this period are located under the dense vines and cover a very small area; therefore, both sources of non-stomatal contributions are likely to be overwhelmed by canopy fluxes because they might be much weaker than their stomatal counterparts, might be decoupled (no E from interrows, just R), or might be recycled by leaf uptake before they reach the instrument levels.

The ratio T/ET , computed by CEC and MREA, is close to unity during the green foliage phase (Fig. 8). While it is expected that evaporation would be smaller given that it is a dry period and the drip irrigation system is an economic technique (and irrigation lines are located under the vines, in the shaded region), it is not possible to affirm, without independent estimates, that E is truly negligible. In a similar vineyard also part of the GRAPEX, Kustas et al. (2019) found temporal and spatial variability in radiation received in the interrow and below canopy and reported that although soil evaporation is less important than transpiration, it is not negligible (they used micro-Bowen ratio systems).

A closer inspection of the quadrant plots between c' and q' during the green foliage phase (figures not shown) indicated a nearly perfect anti-correlation in the middle of the day. This result is also clear in Fig. 7, which shows the diurnal average of $\rho_{c,q'}$. The proportionality between CO_2 and H_2O fluctuations and the high correlation suggests that both scalars are similarly transported (Hill, 1989). Similarity would be expected in this case if the pairs of flux components are consistently correlated/anti-correlated in all sinks and sources (Li and Bou-Zeid, 2011; Li et al., 2012), or if the sampling height is outside the roughness sublayer. Thus, another plausible and likely explanation for the small soil flux estimates is that the height of the eddy-covariance system is located too far from the canopy (similar to what was verified above the canopy at the MP site), causing air parcels carrying the weak soil flux fingerprint to be completely mixed with that from the stronger canopy components before arriving at the sensor.

Overall, the implementation of the partitioning methods during the green phase over the vineyard highlights the most important assumptions and weaknesses of the methods. While we cannot point to the main cause of these results for CEC and MREA (or how accurate they are), we can indicate conditions that are likely to impact their performance. Note that our results do not allow for evaluating the performance of the FVS method: it could be overestimating the soil fluxes. Not only do we not have independent estimates to assess these results, but FVS also shares similar assumptions to CEC and MREA that are not testable using conventional field data.

Moving to the transition period, the correlation coefficient $\rho_{c,q}$ drops, indicating a mixture of signatures from stomatal and non-stomatal components, which is captured by all three methods. The ratios T/ET in this period are comparable, ranging from 0.70 (CEC) to 0.72 (MREA). Results for carbon components, on the other hand, show more disparities. In particular, FVS overestimates respiration and photosynthesis relative to the other methods, which again exposes the main challenge of F_c partitioning: because CO_2 components have different directions and signs, potentially resulting in zero net flux, their sum cannot be constrained by the total flux. This complicates the interpretation of results and comparison of different methods when independent estimates of CO_2 flux components are not available. Furthermore, F_c partitioning results are usually noisier than ET results.

The vineyard is devoid of any green vegetation during the bare soil phase. Therefore, we would expect positive carbon dioxide flux dominated by respiration and ET dominated by evaporation, resulting in $\rho_{c,q} \approx +1$. However, as indicated in the last column of Fig. 7, this is not the case. A slightly negative daytime total carbon flux (and $\rho_{c,q} < 0$) indicates that photosynthesis is still present, potentially associated with contamination of the signal from the area outside the vineyard or some vegetation present in the footprint area that is not captured by the phenocam images. Under these conditions, CEC and MREA result in $T/ET \approx 0.55\text{--}0.60$. Although these results are incompatible with the conditions for the area of interest, the negative F_c during the day suggests that photosynthesis and transpiration are captured by the measurements. This highlights the importance of having an adequate footprint representation to obtain reliable flux estimates. The FVS method was not applied in this period because of the absence of leaves (the parameterization of the water-use efficiency requires the definition of the leaf temperature).

4.4.2. WRE forest

The partitioning results over the WRE forest, in Washington, are shown in Fig. 9. The three methods agree to some extent, particularly in case of CEC and MREA. They result in similar flux magnitudes, even for carbon dioxide flux components that usually result in more variability (although carbon fluxes are noisier, which is more evident for FVS). According to CEC, transpiration dominates in all seasons, varying from $T_{CEC}/ET = 0.62$ in the summer to $T_{CEC}/ET = 0.79$ in the spring (Fig. 8). These ratios are in agreement with those reported in the compilation of previous studies performed by Wei et al. (2017). According to Wei et al. (2017)'s summary, needle-leaf forests with an average LAI of $1.4\text{ m}^2\text{ m}^{-2}$ were found to have T/ET ratios ranging from ≈ 0.3 to ≈ 0.8 , with an

average value equal 0.53. The large variability associated with a narrow leaf area index range is likely related to seasonality, but can also be an artifact caused by uncertainties in the different partitioning techniques used in these studies.

According to all three methods, E was greater in summer (around 70 W m^{-2} in the middle of the day), peaking near 100 W m^{-2} in July (monthly results are shown in the supplementary material). Despite summer being a dry period, the volumetric soil water content measured at the surface is high and decreases, almost linearly, from $0.15 \text{ cm}^3 \text{ cm}^{-3}$ at the beginning of July to $0.06 \text{ cm}^3 \text{ cm}^{-3}$ at the end of August. Thus, the large moisture availability, associated with a period of high net radiation and VPD (Fig. 2b), likely resulted in a large evaporation component, accounting for nearly 40% of total ET (according to CEC) during

summer. Following summer, all methods attribute most ET to transpiration during fall and winter ($T/ET \approx 0.62\text{--}0.75$), with the exception of FVS during winter ($T_{FVS}/ET \approx 0.45$). One of the limitations of all methods is related to water intercepted by leaves. Evaporation of water intercepted by leaves may be mistakenly attributed to transpiration if air parcels transported from the canopy are enriched in water vapor from both leaf transpiration and intercepted water evaporation and depleted in carbon due to photosynthesis. Since rainfall events were abundant in both seasons, it is possible that the high estimated transpiration was a combination of leaf transpiration and evaporation of intercepted water.

Regarding carbon dioxide flux components, respiration estimates exhibited less variability across seasons compared to those of photosynthesis. In addition, the greatest discrepancy across methods occurs in

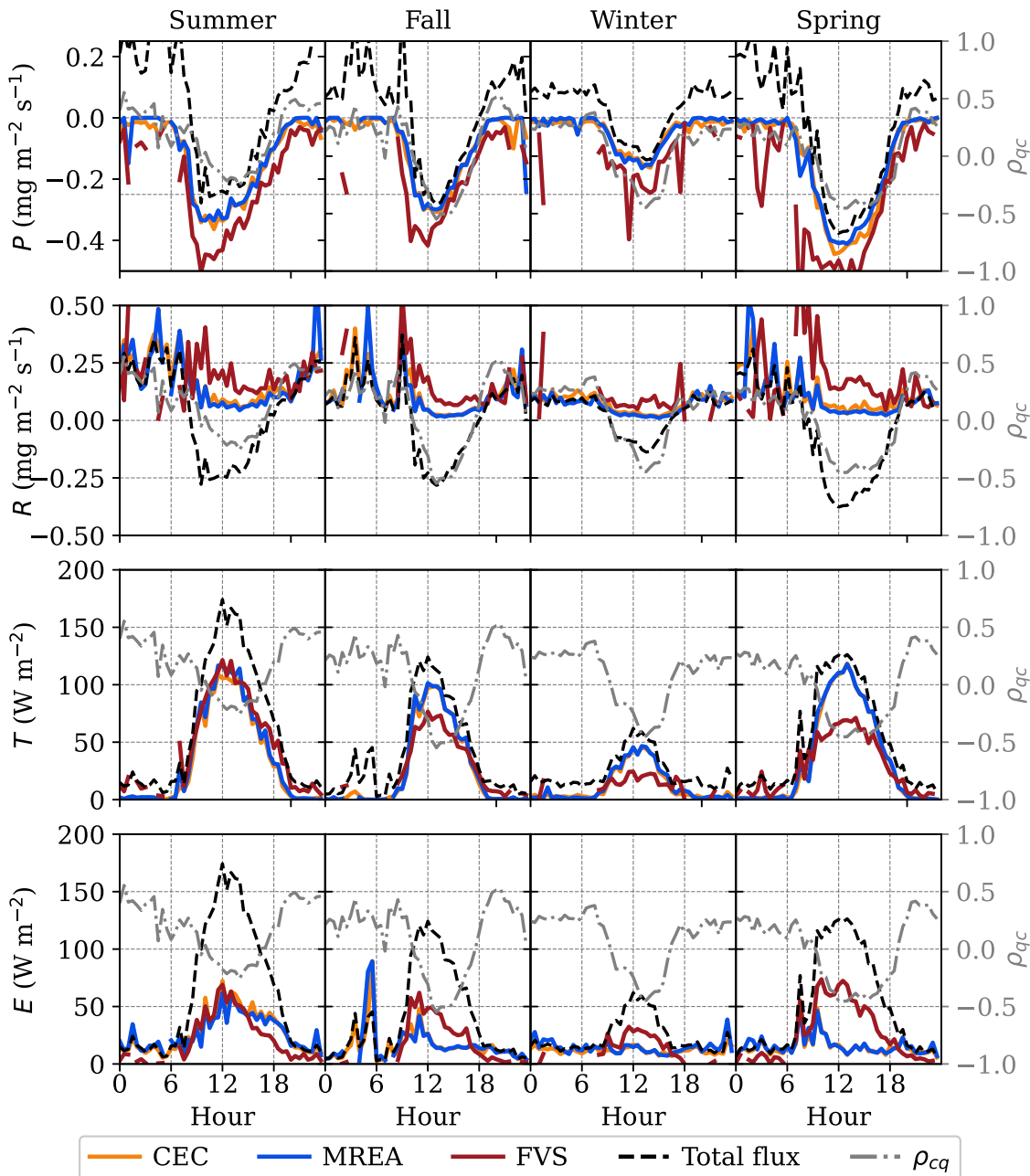


Fig. 9. Comparison of partitioning flux components obtained over the WRE forest in Washington. The average diel cycle during each period is depicted, with dashed black lines representing the total EC fluxes of water and carbon computed using all available data (i.e., it does not exclude data when solutions were not found by one or more of the methods). Summer includes the months of July and August 2018, fall includes September to November 2018, winter includes December 2018 to February 2019, and spring includes March to May 2019.

spring, when FVS yields a much higher R , P , and evaporation relative to the other methods. Again, the dominance of stomatal over non-stomatal components, as found by all methods, is consistent with the negative correlation coefficient.

One important aspect of turbulent transport in forests is the coupling between below and above canopies (Freire et al., 2017; Gerken et al., 2017; Paul-Limoges et al., 2017; Thomas and Foken, 2007; Thomas et al., 2013). All three partitioning methods directly or indirectly assume that they are coupled; that is, the below and above canopy spaces are connected and the EC system above the canopy is able to sample air parcels enriched with respiration carbon emanating from the soil. For the WRE site, a relatively sparse coniferous forest with an LAI of about 1.4 $m^2 m^{-2}$ in July, such assumption is plausible in many of the analyzed periods (except for very stable atmospheric conditions). However, over other types of forests, it may not be valid during some periods of maximum canopy density or conditions of low turbulence under the canopy, as shown by previous authors (Paul-Limoges et al., 2017; Thomas et al., 2013). Another implication of this decoupling is related to carbon dioxide recycling by leaves (Brooks et al., 1997); as the air remains confined in the lower canopy, respiration carbon can be assimilated before it lifts above the tree crowns to be detected by the measurements (Greaver et al., 2005; Knohl et al., 2005; Kondo et al., 2005; Sternberg et al., 1997). Therefore, all methods may underestimate soil respiration if the released carbon dioxide from soil is further assimilated by plants or

not transported by turbulence to the EC level above the canopy. Under such circumstances, any partitioning method that uses EC fluxes (independent of the formulation) will incur uncertainties. To overcome this limitation, previous studies (Paul-Limoges et al., 2017; Thomas et al., 2013) used below and above canopy EC data to investigate turbulent mixing and to identify periods of decoupling, a topic that continues to spawn research interest for ideal and non-ideal conditions alike (Jocher et al., 2020).

4.5. Implications of the assumed coupling between carbon dioxide and water vapor

One consequence of the assumed coupling between carbon dioxide and water vapor fluxes is that all components are required to be non-negligible. For instance, evaporation is tied to respiration since both non-stomatal components are detected in air parcels enriched in carbon and water vapor; therefore, to detect evaporation, respiration should be present. Note that this is not a problem for stomatal components since P and T have to happen simultaneously. In addition, near zero net carbon dioxide flux does not preclude the application of the partitioning methods as long as both photosynthesis and respiration are non-negligible but are balancing each other. However, while CEC can still be applied to ET components in such circumstances, it may not find valid solutions for carbon components when $R/P \approx -1$. Over the grass site,

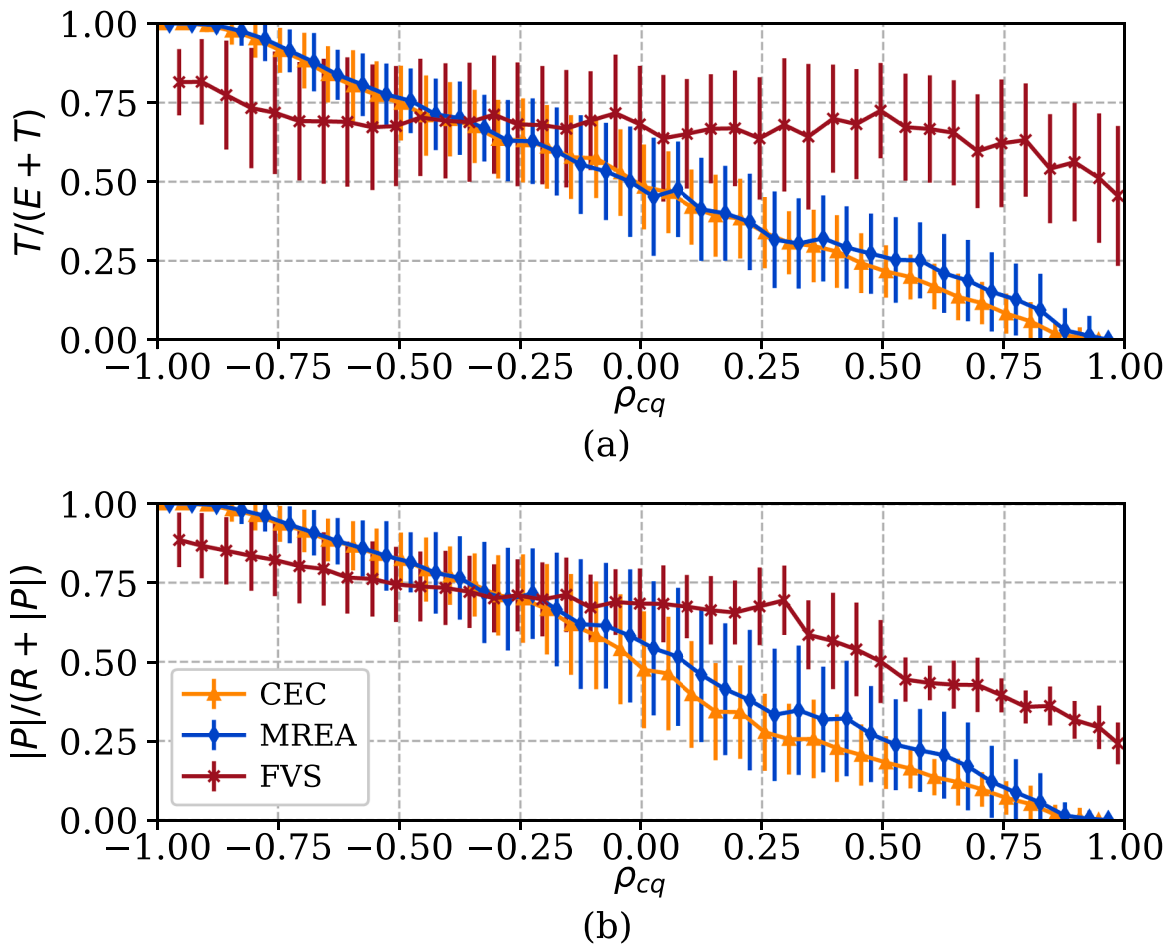


Fig. 10. Correlation coefficient for water vapor and carbon dioxide, $\rho_{c,q}$, versus (a) T/ET and (b) $|P|/(R+|P|)$, with R and P computed using each method. All ratios were computed using half-hourly fluxes from all sites investigated in this paper. Symbols represent the mean of each bin and bars represent one standard deviation. Data during 6 am to 6 pm (local time) for four sites (grass field, MP forest, vineyard and the WRE forest) are included in the figure.

for instance, the method resulted in nonphysical oscillations for R and P when F_c decreased to values in the vicinity of $0.1 \text{ mg CO}_2 \text{ m}^{-2} \text{ s}^{-1}$.

In addition to being non-negligible, the application of the methods require that all flux components have the “expected” direction. In this case, we expect positive water vapor fluxes from the surface to the atmosphere (i.e. no condensation) to be associated with respiration. Although this constraint is physically plausible during the day, negative ET might happen (and was detected more often in the forested sites) due to dew formation during nighttime. However, because daytime conditions are the main focus of interest, the impact of dew formation on the results should only be a concern during winter months or over cold regions.

One challenge for all three methods is the interception of water by leaves. CEC computes transpiration associated with photosynthesis and evaporation linked to respiration (with the exception of leaf respiration, as previously discussed). In this case, if water is being evaporated from leaves or nearby branches at the same time that photosynthesis is occurring, this evaporation will likely be accounted for as transpiration since positive q' will be associated with negative c' . Therefore, care must be taken in interpreting the results of all methods over ecosystems when interception is a large component of the water budget. For example, periods following rainfall events can be removed from the analysis or segregated from other periods.

Perhaps the most important constraint for successful application of partitioning methods based on the similarity between scalars is the measurement height z . More specifically, z must be sufficiently close to the canopy to sample the mixed signal from the different sinks and sources of water vapor and carbon dioxide (Klosterhalfen et al., 2019a; 2019b). If sampling heights are too far from the canopy, turbulence will likely fully mix air parcels emanating from different flux footprints for E and T or P and R , thereby significantly scrambling the signature from soil and vegetation. Under such conditions, the conditional sampling will no longer be robust.

This constraint may preclude the application of such methods in data sets where $z/h \gg 1$, and might suggest that the sensors should be placed just above the canopy height at $z/h \approx 1$. However, this would pose another problem related to measurement inside the roughness sublayer: the signal might be strongly affected by individual canopy elements and thus horizontal homogeneity of the turbulence is likely to be violated. The roughness sublayer is usually estimated to extend up to 2–5h (Cellier and Brunet, 1992; Raupach and Thom, 1981; Thomas et al., 2006), so at present we could offer an empirical recommendation to place the EC system at $z/h \leq 2$. One additional possibility would be the placement of two EC systems, one closer to the canopy, which could be used to obtain the ratios between components needed in Eq. (8), and one EC system further from the canopy, which could ensure converged total fluxes. In any case, further analysis is required to inform a better placement of the sensors. An optimal placement should also consider the effect of canopy density on the flow in the roughness sublayer, as recommended by Klosterhalfen et al. (2019a,b). However, for reasons discussed earlier, data sampled above very dense forests — despite the proximity to the canopy top — are unlikely to yield accurate results.

4.6. Similarity between scalars and partitioning

The framework on which the partitioning methods were derived requires that the stomatal and non-stomatal components are similarly transported by turbulence given their collocated sources and/or sinks. The implication is that the correlation coefficient between CO_2 and H_2O can serve as a measure of the importance of carbon dioxide and water vapor components. Dominance by stomatal components of photosynthesis and transpiration will result in $\rho_{c,q} \approx -1$ given that these fluxes have opposite directions; similarly, $\rho_{c,q} \approx +1$ indicates dominance by

non-stomatal components. Correlation coefficients between these two limits represent intermediate states where all flux components are important.

Fig. 10 shows the ratio $T/(E+T)$ and $|P|/(R+|P|)$ obtained using all three partitioning methods (from half-hourly fluxes) versus $\rho_{c,q}$. Note that we used $R+|P|$ as the denominator instead of F_c in order to set the upper bound of this ratio to unity. In agreement with its theoretical framework, CEC results are strongly related to the correlation coefficient. Transpiration and photosynthesis (evaporation and respiration) dominate when $\rho_{c,q} \approx -1$ ($\rho_{c,q} \approx +1$); when $\rho_{c,q} \approx 0$, the ratio T/ET is in the range 0.50 ± 0.15 . While this is not a substitute for the method, it is a computable and informative measure of the relative importance of transpiration over evaporation.

Note that having $\rho_{c,q} = -1$ will not always indicate dominance by plant flux components. The same applies for $\rho_{c,q} = +1$. As discussed throughout the paper, other factors — such as EC system placement outside the roughness sublayer or over dense canopies — might result in high correlations even in the presence of different sinks and sources of both scalars. Thus, such results must be interpreted in the context of the specificity of the setup.

The MREA method shows a similar trend to CEC, indicating a strong correlation between the flux component ratios and $\rho_{c,q}$. The similar trends are not a surprise given the shared assumptions between both methods. In contrast, FVS results for ET components show a weaker dependence on $\rho_{c,q}$ than the results for F_c components; for instance, for the range from $\rho_{c,q} = -0.5$ to $\rho_{c,q} = +0.5$, $T_{\text{FVS}}/ET \approx 0.7$. This weak dependence is unexpected given that FVS is the only approach that directly uses $\rho_{c,q}$ in its formulation. The ratio $|P_{\text{FVS}}|/(R_{\text{FVS}} + |P_{\text{FVS}}|)$, on the other hand, shows a monotonous decrease with the increase in $\rho_{c,q}$, similar to CEC and MREA.

For both ET and F_c partitioning, CEC and MREA agree well (on average) under most conditions, and they both depart from FVS estimates particularly when non-stomatal components are greater than their stomatal counterparts. FVS also departs from the other two approaches in the limit of weak non-stomatal components ($\rho_{c,q} \approx -1$). The range of moderate negative correlations from $\rho_{c,q} \approx -0.5$ to ≈ -0.15 seems to result in closer CO_2 flux ratios for all three methods; ET components, on the other hand, are more similar in magnitude in a narrower range from $\rho_{c,q} \approx -0.4$ to ≈ -0.15 .

5. Conclusions

Promising methods to partition H_2O and CO_2 fluxes are based on similarity between stomatal (transpiration and photosynthesis) and non-stomatal (evaporation and respiration) pairs of component fluxes. Such formulations combine measured high-frequency carbon dioxide and water vapor EC data and find all four component fluxes simultaneously. Based on this framework, we proposed a new approach, the conditional eddy covariance (CEC), to partition ecosystem fluxes. The CEC method, along with two previously developed techniques — the flux-variance similarity (FVS) and the modified relaxed eddy accumulation (MREA) — were tested against independent estimates of transpiration and soil respiration from a grass site and a forest. These methods’ performance was further investigated over a vineyard and a pine forest across contrasting seasons. The main findings are:

1. The CEC method performed better than MREA and FVS over the grass site in Kenya. It yielded biophysically acceptable results more often and its estimated daily averaged transpiration was highly correlated with both independent estimates from leaf-level measurements ($\rho = 0.96$) and stable isotopes ($\rho = 0.71$). It also resulted in the smallest RMSE ($= 5.9 \text{ W m}^{-2}$) and bias ($= -0.09 \text{ W m}^{-2}$) against T_{LEAF} . In

- terms of CO₂ components, P_{CEC} indicated higher magnitudes in the middle of the two-week experiment, when the green leaf coverage was at its peak.
2. The evaluation of soil respiration computed from all three methods against measurements by chambers at the MP forest resulted in variable performance. R_{FVS} computed above the canopy was closer to R_{CH} than the estimates from CEC and MREA; however, R_{FVS} overestimated R_{CH} in the middle of the canopy. The CEC and MREA methods, on the other hand, performed better below the canopy, where both converged to biophysically acceptable results more frequently and resulted in higher correlations and smaller errors relative to the chamber estimates. Although one must bear in mind that chamber data have their own uncertainty that we cannot quantify.
 3. One main issue regarding the performance of the CEC method is its implementation in conditions of small net CO₂ fluxes when both P and R are non-negligible but nearly balance each other. Under such conditions, noisier R and P estimates are expected. In extreme cases when fluxes are consistently low ($F_c \lesssim 0.1 \text{ mg CO}_2 \text{ m}^{-2} \text{ s}^{-1}$), and P and R are expected to be both non-negligible, the method should be avoided for CO₂ flux partitioning; nonetheless, it can still be used to partition ET fluxes.
 4. The FVS method is more applicable and converges more often to valid physical solutions when the correlation between c' and q' is negative. The sites where fewer solutions were found (grass site and below canopy at the MP forest) were characterized by positive correlations and dominance of soil flux components — in such regimes, the mathematical constraints in Eq. (4) were usually not satisfied. The MREA method also has a higher rate of convergence when plant components are important: most of the cases when the method did not converge were nighttime hours or situations when R and/or E were large.
 5. Because of the coupling between carbon dioxide and water vapor, non-negligible fluxes of both soil components are required. Therefore, CEC (also MREA and FVS) requires that soil respiration be occurring simultaneously (and be spatially collocated) with evaporation. Another limitation of all three formulations is related to evaporation from water intercepted by leaves. In this case, evaporation can be erroneously attributed to transpiration if photosynthesis is simultaneously happening.
 6. One of the most important factors to take into account in the implementation of these methods is the measurement height relative to the height of the scalar sinks and sources. Air parcels emanating from the soil surface and canopy air space should not be completely mixed for these methods to be applicable. Thus, measurements should be obtained as close as possible to the canopy top. EC based partitioning methods are also likely to fail above very dense forests where the air layers below and above canopies are decoupled. Although these limitations can prevent the application of these methods at some sites, they can also be circumvented in future experiments when designing the EC system site and position.
 7. The correlation coefficient between carbon dioxide and water vapor fluctuations is an adequate qualitative measure of the relative importance of stomatal over non-stomatal components according to CEC and MREA. Both methods showed a strong relation between T/ET and $\rho_{c,q}$, which is in agreement with the theoretical framework on which they were formulated. For FVS, on the other hand, the ratios of F_c components were more dependent on $\rho_{c,q}$ than the ratios of ET components. Overall, $\rho_{c,q}$ can also be used as an indicator of when the various methods converge or diverge in their estimates, albeit more investigation is needed along these lines.
- More broadly, the investigation of CEC, MREA, and FVS methods over four sites elucidated the main weaknesses and strengths of these approaches, and yielded findings on the conditions under which they (dis)agree. The tests are not intended to find the best or most accurate method, and indeed the results indicate that the three methods taken collectively may be more useful than any single approach. For example, conditions under which all methods find solutions that agree might be optimal for obtaining reliable flux results to understand ecosystem function under a set of restricted conditions. On the other hand, for long term (e.g., annual) water or carbon budgets, it might be advantageous to accept the results even when only a single method yields realistic partitioning to maximize the availability and representativity of flux data (and minimize gap-filling). The present findings can guide such efforts to use these approaches, and indicate important limitations and best practices for their implementation. However, further testing and additional comparisons across all methods remain needed to characterize their constraints. Thus, we recommend that future investigations of this class of partitioning approaches implement all three methods simultaneously. Field experiments designed specifically for this purpose, with EC systems at multiple heights below and above the canopy and independent measurements of at least some of the components, would be valuable to establish best practices and allow wider and more robust application of flux partitioning from high frequency turbulence data.

Data Statement

The data generated during the current study are available from the corresponding author. The raw datasets for the grass site, the vineyard, and the MP forest can be requested from the respective principal investigator. Data from the WRE forest is publicly available and can be downloaded from www.neonscience.org. A python code containing all three partitioning methods is available at <https://github.com/einaraz/PartitioningMethods>.

Declaration of Competing Interest

The authors declare that they have no known competing financial interests or personal relationships that could have appeared to influence the work reported in this paper.

Acknowledgement

E.Z. and E.B.Z are supported by the Moore Charitable Foundation Science-to-Action Fund from the School of Engineering and Applied Science at Princeton and by the Army Research Office under contract W911NF2010216 (program manager Julia Barzyk). S.P.G. acknowledges NSF grant DEB 1802885. G.K. acknowledges support from the U.S. National Science Foundation (NSF-AGS-1644382, NSF-AGS-2028633, and NSF-IOS-1754893). C.K.T. acknowledges support from the U.S. National Science Foundation (NSF-AGS-0955444) and the European Research Council (ERC) under the European Unions Horizon 2020 research and innovation programme (grant agreement no. 724629). N.L.D. acknowledges Brazils National Research Council (CNPq) research scholarship 301420/2017-3. B.K. acknowledges funding and logistical support from E. & J. Gallo Winery and from the NASA Applied Sciences-Water Resources Program (Grant No. NNH17AE39I) for the vineyard data used in this study as part of the GRAPEX project. In addition, we thank the staff of Viticulture, Chemistry and Enology Division of E. & J. Gallo Winery and the cooperation of the vineyard management staff at the Ripperdan Ranch for supporting the field measurements. USDA is an equal opportunity provider and employer. Z.G. acknowledges the National Natural Science Foundation of China (41875013). We thank the reviewers and the editor for their detailed and thoughtful comments, which helped improve the paper.

Appendix A. Details on the implementation of FVS

1. Additional equations of the Flux Variance Similarity method

To solve Eq. (3a) and (3b), the variance of c_p , σ_{cp}^2 , and the correlation coefficient between c_p and c_r , ρ_{c_p, c_r} , are needed. These turbulence statistics are computed by the following expressions (Palatella et al., 2014; Scanlon et al., 2019)

$$\sigma_{cp}^2 = \frac{\left(1 - \rho_{c,q}^2\right)(\sigma_q \sigma_c W)^2 \left(\sigma_q^2 \overline{w' c'}^2 - 2\rho_{c,q} \sigma_q \sigma_c \overline{w' c'} \overline{w' q'} + \sigma_c^2 \overline{w' q'}^2\right)}{\left[\sigma_c^2 \overline{w' q'} + \sigma_q^2 \overline{w' c'} W - \rho_{c,q} \sigma_q \sigma_c (\overline{w' c'} + \overline{w' q'} W)\right]^2}, \quad (\text{A.1})$$

$$\rho_{cp, cr}^2 = \frac{\left(1 - \rho_{c,q}^2\right) \sigma_q^2 \sigma_c^2 (\overline{w' c'} - \overline{w' q'} W)^2}{\left(\sigma_q^2 \overline{w' c'}^2 - 2\rho_{c,q} \sigma_q \sigma_c \overline{w' q'} \overline{w' c'} + \sigma_c^2 \overline{w' q'}^2\right) \left(\sigma_c^2 - 2\rho_{c,q} \sigma_q \sigma_c W + \sigma_q^2 W^2\right)}. \quad (\text{A.2})$$

2. Convergence of partitioning methods

Tables A1 and A2 provide further details on the main constraints or reasons for the non-convergence of the three methods.

Table A1

Percentage of the total half-hourly periods for which a valid solution was found by each partitioning method at the MP forest site. The three most common causes of discarded solutions for each method are also shown. For both CEC and FVS, the solution is discarded whenever the ratio between respiration and photosynthesis, r_{Fc} , is close to -1 . Note that not all constraints apply to all methods. The original available data already discarded nonstationary periods and cases when $ET < 0$.

	MP below			MP mid			MP above		
	CEC	REA	FVS	CEC	REA	FVS	CEC	REA	FVS
Valid solution	99.7	32.0	1.8	82.5	88.8	60.4	97.7	69.8	49.8
$E > ET$ or $P > 0$	—	68.0	—	—	11.1	—	—	30.0	—
Constraint Eq. (4) not met	—	—	97.2	—	—	30.3	—	—	44.7
$-0.8 < r_{Fc} < -1.2$	0.3	—	0.9	17.5	—	9.3	2.3	—	5.5

Table A2

Same as Table A1 for the grassland in Kenya, Vineyard in California, and WRE forest in Washington.

	Grassland			Vineyard			WRE forest		
	CEC	REA	FVS	CEC	REA	FVS	CEC	REA	FVS
Valid solution	94.6	28.9	1.5	98.9	87.9	47.2	97.6	77.9	49.5
$E > ET$ or $P > 0$	—	71.0	—	—	12.0	—	—	22.0	—
Constraint Eq. (4) not met	—	—	97.0	—	—	49.6	—	—	43.5
$-0.8 < r_{Fc} < -1.2$	5.4	—	1.5	1.1	—	2.6	2.4	—	5.5

3. Parameterization of intercellular CO₂ concentration

The water-use efficiency (*WUE*) is a necessary variable to the FVS method. If not known (from measurements, for instance), it needs to be estimated. In our implementation, we obtained five estimates of *WUE* for each half-hour period. Consequently, five estimates of each flux component (later averaged) were obtained.

The first four estimates of *WUE* were obtained by implementing Eq. (5) with different formulations for \bar{c}_s , the intercellular carbon dioxide concentration. The fifth estimate of *WUE* was obtained from a recent optimization model proposed by Scanlon et al. (2019). In the open-source Python module developed by Skaggs et al. (2018), the authors implemented all five models as options to compute the water-use efficiency and the flux components by the FVS method.

The simplest approach to solve Eq. (5) is to use a constant value for \bar{c}_s relative to \bar{c}_c . In our analyses, we used $\bar{c}_s = 280 \mu\text{mol mol}^{-1}$ for C3 plants and $130 \mu\text{mol mol}^{-1}$ for C4 plants (Campbell and Norman, 1998, p. 150). Following Skaggs et al. (2018), we also computed *WUE* by assuming that the ratio \bar{c}_s / \bar{c}_c is constant and equal 0.7 for C3 and $\bar{c}_s / \bar{c}_c = 0.44$ for C4 plants (Sinclair et al., 1984).

The third formulation of \bar{c}_s follows the linear relation between \bar{c}_s / \bar{c}_c and water vapor pressure deficit D (based on the leaf-temperature, here assumed to be saturated conditions at the air temperature), obtained by Morison and Gifford (1983),

$$\frac{\bar{c}_s}{\bar{c}_c} = a - bD, \quad (\text{A.3})$$

where $a = 1$ and $b = 1.6 \times 10^{-4} \text{ Pa}^{-1}$ or $b = 2.7 \times 10^{-4} \text{ Pa}^{-1}$ for C3 and C4 plants (Skaggs et al., 2018), respectively. Finally, we also implemented a second formulation that relates \bar{c}_s / \bar{c}_c to the square root of D (Katul et al., 2009),

$$\frac{\bar{c}_s}{\bar{c}_a} = 1 - \sqrt{\frac{\alpha \lambda D}{\bar{c}_a}}, \quad (\text{A.4})$$

where $\alpha = 1.6$ is the relative diffusivity of water with respect to carbon. This formulation is based on stomatal optimization theories that maximize carbon gain for a given loss of water from leaves assuming Rubisco limits photosynthesis. We used $\lambda = 22 \times 10^{-9}$ kg CO₂ m⁻³ Pa⁻¹ (Skaggs et al., 2018), though λ does vary with the soil moisture state as discussed elsewhere (Mrad et al., 2019).

Appendix B. FVS results for different WUE parameterizations

Fig. B1 shows the diurnal cycle of the four flux components — as found by the five parameterizations of the WUE — according to the FVS method. Figures shown only for the green foliage phase at the vineyard (a) and spring at the WRE forest (b).

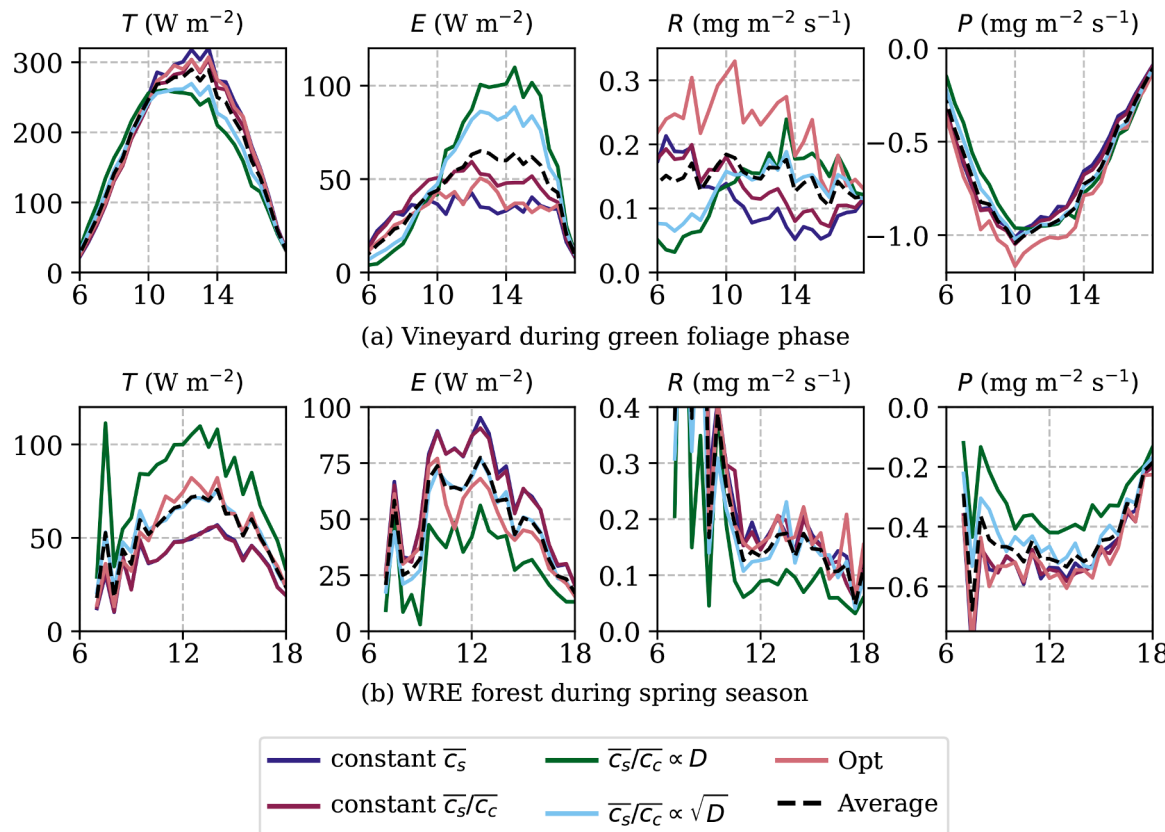


Fig. B1. Diurnal cycles for FVS results during the green foliage phase at the vineyard (a) and during the spring season at the WRE forest (b). The diurnal cycles of flux components for five different parameterizations for WUE, as well as the average diurnal cycle, are shown. In the legend, Opt refers to the optimization model proposed by Scanlon et al. (2019). A description of the remaining models is given in Appendix A. (For interpretation of the references to colour in this figure legend, the reader is referred to the web version of this article.)

Supplementary material

Supplementary material associated with this article can be found, in the online version, at doi:[10.1016/j.agrformet.2021.108790](https://doi.org/10.1016/j.agrformet.2021.108790)

References

- Baker, J., Norman, J., Bland, W., 1992. Field-scale application of flux measurement by conditional sampling. *Agric For Meteorol* 62 (1–2), 31–52.
- Baker, J.M., 2000. Conditional sampling revisited. *Agric For Meteorol* 104 (1), 59–65.
- Brooks, J.R., Flanagan, L.B., Varney, G.T., Ehleringer, J.R., 1997. Vertical gradients in photosynthetic gas exchange characteristics and refixation of respired CO₂ within boreal forest canopies. *Tree Physiol.* 17 (1), 1–12. <https://doi.org/10.1093/treephys/17.1.1>.
- Campbell, G.S., Norman, J.M., 1998. An Introduction to Environmental Biophysics. Springer, New York, NY. <https://doi.org/10.1007/978-1-4612-1626-1>.
- Cellier, P., Brunet, Y., 1992. Flux-gradient relationships above tall plant canopies. *Agric For Meteorol* 58 (1), 93–117. [https://doi.org/10.1016/0168-1923\(92\)90113-I](https://doi.org/10.1016/0168-1923(92)90113-I).
- Detto, M., Katul, G., Mancini, M., Montaldo, N., Albertson, J., 2008. Surface heterogeneity and its signature in higher-order scalar similarity relationships. *Agric For Meteorol* 148 (6–7), 902–916.
- Detto, M., Katul, G.G., 2007. Simplified expressions for adjusting higher-order turbulent statistics obtained from open path gas analyzers. *Boundary Layer Meteorol* 122, 1472–1573. <https://doi.org/10.1007/s10546-006-9105-1>.
- Foken, T., 2017. Micrometeorology. Springer-Verlag Berlin Heidelberg. <https://doi.org/10.1007/978-3-642-25440-6>.
- Freire, L.S., Gerken, T., Ruiz-Plancarte, J., Wei, D., Fuentes, J.D., Katul, G.G., Dias, N.L., Acevedo, O.C., Chamecki, M., 2017. Turbulent mixing and removal of ozone within an amazon rainforest canopy. *Journal of Geophysical Research: Atmospheres* 122 (5), 2791–2811. <https://doi.org/10.1002/2016JD026009>.
- Gerken, T., Chamecki, M., Fuentes, J.D., 2017. Air-parcel residence times within forest canopies. *Boundary Layer Meteorol* 165 (1), 29–54. <https://doi.org/10.1007/s10546-017-0269-7>.

- Good, S.P., Soderberg, K., Guan, K., King, E.G., Scanlon, T.M., Caylor, K.K., 2014. $\delta_2\text{H}$ isotopic flux partitioning of evapotranspiration over a grass field following a water pulse and subsequent dry down. *Water Resour Res* 50 (2), 1410–1432. <https://doi.org/10.1002/2013WR014333>.
- Greaver, T., da Silveira Lobo Sternberg, L., Schaffer, B., Moreno, T., 2005. An empirical method of measuring CO_2 recycling by isotopic enrichment of respired CO_2 . *Agric For Meteorol* 128 (1), 67–79. <https://doi.org/10.1016/j.agrformet.2004.08.007>.
- Hill, R.J., 1989. Implications of Monin-Obukhov similarity theory for scalar quantities. *Journal of Atmospheric Sciences* 46 (14), 2236–2244. [https://doi.org/10.1175/1520-0469\(1989\)046<2236:IOMSTF>2.0.CO;2](https://doi.org/10.1175/1520-0469(1989)046<2236:IOMSTF>2.0.CO;2).
- Irvine, J., Law, B.E., 2002. Contrasting soil respiration in young and old-growth ponderosa pine forests. *Glob Chang Biol* 8 (12), 1183–1194. <https://doi.org/10.1046/j.1365-2486.2002.00544.x>.
- Irvine, J., LAW, B.E., Martin, J.G., Vickers, D., 2008. Interannual variation in soil CO_2 efflux and the response of root respiration to climate and canopy gas exchange in mature ponderosa pine. *Glob Chang Biol* 14 (12), 2848–2859. <https://doi.org/10.1111/j.1365-2486.2008.01682.x>.
- Jocher, G., Fischer, M., Sigut, L., Pavelka, M., Sedlák, P., Katul, G., 2020. Assessing decoupling of above and below canopy air masses at a norway spruce stand in complex terrain. *Agric For Meteorol* 294, 108149.
- Katul, G., Albertson, J., Chu, C.-R., Parlange, M., Stricker, H., Tyler, S., 1994. Sensible and latent heat flux predictions using conditional sampling methods. *Water Resour Res* 30 (11), 3053–3059.
- Katul, G.G., Ellsworth, D.S., Lai, C.-T., 2000. Modelling assimilation and intercellular CO_2 from measured conductance: a synthesis of approaches. *Plant, Cell & Environment* 23 (12), 1313–1328. <https://doi.org/10.1046/j.1365-3040.2000.00641.x>.
- Katul, G.G., Finkelstein, P.L., Clarke, J.F., Ellestad, T.G., 1996. An investigation of the conditional sampling method used to estimate fluxes of active, reactive, and passive scalars. *Journal of Applied Meteorology and Climatology* 35 (10), 1835–1845.
- Katul, G.G., Palmroth, S., Oren, R., 2009. Leaf stomatal responses to vapour pressure deficit under current and CO_2 -enriched atmosphere explained by the economics of gas exchange. *Plant, Cell & Environment* 32 (8), 968–979. <https://doi.org/10.1111/j.1365-3040.2009.01977.x>.
- Klosterhalfen, A., Graf, A., Brüggemann, N., Drüe, C., Esser, O., González-Dugo, M.P., Heinemann, G., Jacobs, C.M.J., Mauder, M., Moene, A.F., Ney, P., Pütz, T., Rebmann, C., Ramos Rodríguez, M., Scanlon, T.M., Schmidt, M., Steinbrecher, R., Thomas, C.K., Valler, V., Zeeman, M.J., Vereecken, H., 2019. Source partitioning of H_2O and CO_2 fluxes based on high-frequency eddy covariance data: a comparison between study sites. *Biogeosciences* 16 (6), 1111–1132. <https://doi.org/10.5194/bg-16-1111-2019>.
- Klosterhalfen, A., Moene, A., Schmidt, M., Scanlon, T., Vereecken, H., Graf, A., 2019. Sensitivity analysis of a source partitioning method for H_2O and CO_2 fluxes based on high frequency eddy covariance data: findings from field data and large eddy simulations. *Agric For Meteorol* 265, 152–170. <https://doi.org/10.1016/j.agrformet.2018.11.003>.
- Knipper, Kustas, Anderson, Alsina, Hain, Alfieri, Prueger, Gao, McKee, Sanchez, 2019. Using high-spatiotemporal thermal satellite retrievals for operational water use and stress monitoring in a California vineyard. *Remote Sens (Basel)* 11 (18), 2124. <https://doi.org/10.3390/rs11182124>.
- Knohl, A., Werner, R.A., Brand, W.A., Buchmann, N., 2005. Short-term variations in CO_2 of ecosystem respiration reveals link between assimilation and respiration in a deciduous forest. *Oecologia* 142 (1), 70–82. <https://doi.org/10.1007/s00442-004-1702-4>.
- Kondo, M., Muraoka, H., Uchida, M., Yazaki, Y., Koizumi, H., 2005. Refixation of respired CO_2 by understory vegetation in a cool-temperate deciduous forest in Japan. *Agric For Meteorol* 134 (1), 110–121. <https://doi.org/10.1016/j.agrformet.2005.10.006>.
- Kool, D., Agam, N., Lazarovitch, N., Heitman, J., Sauer, T., Ben-Gal, A., 2014. A review of approaches for evapotranspiration partitioning. *Agric For Meteorol* 184, 56–70. <https://doi.org/10.1016/j.agrformet.2013.09.003>.
- Koskinen, M., Minkkinen, K., Ojanen, P., Kämäräinen, M., Laurila, T., Lohila, A., 2014. Measurements of CO_2 exchange with an automated chamber system throughout the year: challenges in measuring night-time respiration on porous peat soil. *Biogeosciences* 11 (2), 347–363. <https://doi.org/10.5194/bg-11-347-2014>.
- Kostner, B., Falge, E., Alsheimer, M., 2017. Sap Flow Measurement. In: Foken, T. (Ed.), *Energy and Matter Fluxes of a Spruce Forest Ecosystem. Ecological Studies (Analysis and Synthesis)*. Springer, pp. 99–116.
- Kustas, W.P., Agam, N., Alfieri, J.G., McKee, L.G., Prueger, J.H., Higgs, L.E., Howard, A.M., Heitman, J.L., 2019. Below canopy radiation divergence in a vineyard: implications on interrow surface energy balance. *Irrigation Science* 37 (3), 227–237.
- Kustas, W.P., Anderson, M.C., Alfieri, J.G., Knipper, K., Torres-Rua, A., Parry, C.K., Nieto, H., Agam, N., White, W.A., Gao, F., McKee, L., Prueger, J.H., Higgs, L.E., Los, S., Alsina, M.M., Sanchez, L., Sams, B., Dokoozlian, N., McKee, M., Jones, S., Yang, Y., Wilson, T.G., Lei, F., McElrone, A., Heitman, J.L., Howard, A.M., Post, K., Melton, F., Hain, C., 01 Sep. 2018. The grape remote sensing atmospheric profile and evapotranspiration experiment. *Bull. Am. Meteorol. Soc.* 99 (9), 1791–1812. <https://doi.org/10.1175/BAMS-D-16-0244.1>.
- Lee, S.-C., Christen, A., Black, T.A., Jassal, R.S., Ketler, R., Nesic, Z., 2020. Partitioning of net ecosystem exchange into photosynthesis and respiration using continuous stable isotope measurements in a pacific northwest douglas-fir forest ecosystem. *Agric For Meteorol* 292–293, 108109. <https://doi.org/10.1016/j.agrformet.2020.108109>.
- Li, D., Bou-Zeid, E., 2011. Coherent structures and the dissimilarity of turbulent transport of momentum and scalars in the unstable atmospheric surface layer. *Boundary Layer Meteorol* 140 (2), 243–262. <https://doi.org/10.1007/s10546-011-9613-5>.
- Li, D., Bou-Zeid, E., de Bruin, H.A., 2012. Monin-Obukhov similarity functions for the structure parameters of temperature and humidity. *Boundary Layer Meteorol* 145 (1), 45–67. <https://doi.org/10.1007/s10546-011-9660-y>.
- Li, X., Gentine, P., Lin, C., Zhou, S., Sun, Z., Zheng, Y., Liu, J., Zheng, C., 2019. A simple and objective method to partition evapotranspiration into transpiration and evaporation at eddy-covariance sites. *Agric For Meteorol* 265, 171–182. <https://doi.org/10.1016/j.agrformet.2018.11.017>.
- Ma, S., Eichelmann, E., Wolf, S., Rey-Sánchez, C., Baldocchi, D.D., 2020. Transpiration and evaporation in a californian oak-grass savanna: field measurements and partitioning model results. *Agric For Meteorol* 295, 108204. <https://doi.org/10.1016/j.agrformet.2020.108204>.
- Metzger, S., Durden, D., Florian, C., Luo, H., Pinginha-Durden, N., Xu, K., 2018. NEON Algorithm Theoretical Basis Document (ATBD): eddy-covariance data products bundle. Technical Report. National Ecological Observatory Network.
- Misson, L., Baldocchi, D., Black, T., Blanken, P., Brunet, Y., Curiel Yuste, J., Dorsey, J., Falk, M., Granier, A., Irvine, M., Jarosz, N., Lamaud, E., Launiainen, S., Law, B., Longdoz, B., Loustau, D., McKay, M., Paw U, K., Vesala, T., Vickers, D., Wilson, K., Goldstein, A., 2007. Partitioning forest carbon fluxes with overstory and understory eddy-covariance measurements: a synthesis based on fluxnet data. *Agric For Meteorol* 144 (1), 14–31. <https://doi.org/10.1016/j.agrformet.2007.01.006>.
- Morison, J.I.L., Gifford, R.M., 1983. Stomatal sensitivity to carbon dioxide and humidity. *Plant Physiol.* 71 (4), 789–796. <https://doi.org/10.1104/pp.71.4.789>.
- Mrad, A., Sevanto, S., Domèc, J.-C., Liu, Y., Nakad, M., Katul, G., 2019. A dynamic optimality principle for water use strategies explains isohydric to anisohydric plant responses to drought. *Frontiers in Forests and Global Change* 2, 49.
- National Ecological Observatory Network, 2020a. Data product dp4.00200.001, bundled data products - eddy covariance. Provisional data downloaded from <http://data.neonscience.org> on August 7, 2020. Battelle, Boulder, CO, USA NEON. 2020.
- National Ecological Observatory Network, 2020b. Wind river experimental forest-wref. <https://www.neonscience.org/field-sites/wref>. Accessed: 2020-12-15.
- National Ecological Observatory Network, 2021a. Data product dp1.00006.001, precipitation. Provisional data downloaded from <http://data.neonscience.org> on January 21, 2021. Battelle, Boulder, CO, USA NEON. 2021.
- National Ecological Observatory Network, 2021b. Data product dp1.00023.001, shortwave and longwave radiation (net radiometer). Provisional data downloaded from <http://data.neonscience.org> on January 21, 2021. Battelle, Boulder, CO, USA NEON. 2021.
- National Ecological Observatory Network, 2021c. Data product dp1.00033.001, phenology images. Provisional data downloaded from <http://data.neonscience.org> on January 18, 2021. Battelle, Boulder, CO, USA NEON. 2021.
- National Ecological Observatory Network, 2021d. Data product dp1.00094.001, soil water content and water salinity. Provisional data downloaded from <http://data.neonscience.org> on January 20, 2021. Battelle, Boulder, CO, USA NEON. 2021.
- National Ecological Observatory Network, 2021e. LAI - spectrometer - flightline (dp2.30012.001). https://data.neonscience.org/data-products/DP2.30012.001/REL_EASE-2021_10.48443/ABRM-BS86.
- National Ecological Observatory Network, 2021f. NEON data products. <https://data.neonscience.org/data-products/explore>. Accessed: 2021-01-26.
- Nelson, J.A., Carvalhais, N., Cuntz, M., Delpierre, N., Knauer, J., Ogée, J., Migliavacca, M., Reichstein, M., Jung, M., 2018. Coupling water and carbon fluxes to constrain estimates of transpiration: the tea algorithm. *Journal of Geophysical Research: Biogeosciences* 123 (12), 3617–3632. <https://doi.org/10.1029/2018JG004727>.
- Nilson, T., 1971. A theoretical analysis of the frequency of gaps in plant stands. *Agricultural Meteorology* 8, 25–38. [https://doi.org/10.1016/0002-1571\(71\)90092-6](https://doi.org/10.1016/0002-1571(71)90092-6).
- Palatella, L., Rana, G., Vitale, D., 2014. Towards a flux-partitioning procedure based on the direct use of high-frequency eddy-covariance data. *Boundary Layer Meteorol* 153, 327–337. <https://doi.org/10.1007/s10546-014-9947-x>.
- Pattey, E., Desjardins, R.L., Rochette, P., 1993. Accuracy of the relaxed eddy-accumulation technique, evaluated using CO_2 flux measurements. *Boundary Layer Meteorol* 66, 341–355. <https://doi.org/10.1007/BF00712728>.
- Paul-Limoges, E., Wolf, S., Eugster, W., Hnrtnagl, L., Buchmann, N., 2017. Below-canopy contributions to ecosystem CO_2 fluxes in a temperate mixed forest in switzerland. *Agric For Meteorol* 247, 582–596. <https://doi.org/10.1016/j.agrformet.2017.08.011>.
- Paul-Limoges, E., Wolf, S., Schneider, F.D., Longo, M., Moorcroft, P., Gharun, M., Damm, A., 2020. Partitioning evapotranspiration with concurrent eddy covariance measurements in a mixed forest. *Agric For Meteorol* 280, 107786. <https://doi.org/10.1016/j.agrformet.2019.107786>.
- Peddiinti, S.R., Kambhammettu, B.P., 2019. Dynamics of crop coefficients for citrus orchards of central india using water balance and eddy covariance flux partition techniques. *Agric. Water Manage.* 212, 68–77. <https://doi.org/10.1016/j.agwat.2018.08.027>.
- Perez-Priego, O., Katul, G., Reichstein, M., El-Madany, T.S., Ahrens, B., Carrara, A., Scanlon, T.M., Migliavacca, M., 2018. Partitioning eddy covariance water flux components using physiological and micrometeorological approaches. *Journal of Geophysical Research: Biogeosciences* 123 (10), 3353–3370. <https://doi.org/10.1029/2018JG004637>.
- Poggi, D., Porporato, A., Ridolfi, L., Albertson, J., Katul, G., 2004. The effect of vegetation density on canopy sub-layer turbulence. *Boundary Layer Meteorol* 111 (3), 565–587.
- Rana, G., Palatella, L., Scanlon, T.M., Martinelli, N., Ferrara, R.M., 2018. CO_2 and H_2O flux partitioning in a mediterranean cropping system. *Agric For Meteorol* 260–261, 118–130. <https://doi.org/10.1016/j.agrformet.2018.06.007>.

- Raupach, M., Thom, A.S., 1981. Turbulence in and above plant canopies. *Annu Rev Fluid Mech* 13 (1), 97–129.
- Rebmann, C., Kolle, O., Heinesch, B., Queck, R., Ibrom, A., Aubinet, M., 2012. Data Acquisition and Flux Calculations. In: Aubinet, M., Vesala, T., Papale, D. (Eds.), *Eddy Covariance: A Practical Guide to Measurement and Data Analysis*. Springer Netherlands, pp. 59–85.
- Reichstein, M., Falge, E., Baldocchi, D., Papale, D., Aubinet, M., Berbigier, P., Bernhofer, C., Buchmann, N., Gilmanov, T., Granier, A., Grönwald, T., Havrankov, K., Ilvesniemi, H., Janous, D., Knohl, A., Laurila, T., Lohila, A., Loustau, D., Matteucci, G., Meyers, T., Miglietta, F., Ourcival, J.-M., Pumpanen, J., Rambal, S., Rotenberg, E., Sanz, M., Tenhunen, J., Seufert, G., Vaccari, F., Vesala, T., Yakir, D., Valentini, R., 2005. On the separation of net ecosystem exchange into assimilation and ecosystem respiration: review and improved algorithm. *Glob Chang Biol* 11 (9), 1424–1439. <https://doi.org/10.1111/j.1365-2486.2005.001002.x>.
- Roupsard, O., Bonnefond, J.-M., Irvine, M., Berbigier, P., Nouvellon, Y., Dauzat, J., Taga, S., Hamel, O., Jourdan, C., Saint-André, L., Miale-Serra, I., Labouisse, J.-P., Epron, D., Joffre, R., Braconier, S., Rouzière, A., Navarro, M., Boullet, J.-P., 2006. Partitioning energy and evapo-transpiration above and below a tropical palm canopy. *Agric For Meteorol* 139 (3), 252–268. <https://doi.org/10.1016/j.agrformat.2006.07.006>.
- Scanlon, T.M., Albertson, J.D., 2001. Turbulent transport of carbon dioxide and water vapor within a vegetation canopy during unstable conditions: identification of episodes using wavelet analysis. *Journal of Geophysical Research: Atmospheres* 106 (D7), 7251–7262. <https://doi.org/10.1029/2000JD900662>.
- Scanlon, T.M., Kustas, W.P., 2010. Partitioning carbon dioxide and water vapor fluxes using correlation analysis. *Agric For Meteorol* 150 (1), 89–99. <https://doi.org/10.1016/j.agrformat.2009.09.005>.
- Scanlon, T.M., Sahu, P., 2008. On the correlation structure of water vapor and carbon dioxide in the atmospheric surface layer: a basis for flux partitioning. *Water Resour Res* 44 (10). <https://doi.org/10.1029/2008WR006932>.
- Scanlon, T.M., Schmidt, D.F., Skaggs, T.H., 2019. Correlation-based flux partitioning of water vapor and carbon dioxide fluxes: method simplification and estimation of canopy water use efficiency. *Agric For Meteorol* 279, 107732. <https://doi.org/10.1016/j.agrformat.2019.107732>.
- Scott, R.L., Biederman, J.A., 2017. Partitioning evapotranspiration using long-term carbon dioxide and water vapor fluxes. *Geophys Res Lett* 44 (13), 6833–6840. <https://doi.org/10.1002/2017GL074324>.
- Sinclair, T.R., Tanner, C.B., Bennett, J.M., 1984. Water-use efficiency in crop production. *Bioscience* 34 (1), 36–40. <http://www.jstor.org/stable/1309424>
- Skaggs, T., Anderson, R., Alfieri, J., Scanlon, T., Kustas, W., 2018. Fluxpart: open source software for partitioning carbon dioxide and water vapor fluxes. *Agric For Meteorol* 253–254, 218–224. <https://doi.org/10.1016/j.agrformat.2018.02.019>.
- Sternberg, L., Moreira, M.Z., Martinelli, L.A., Victoria, R.L., Barbosa, E.M., Bonates, L.C., Nepstad, D.C., 1997. Carbon dioxide recycling in two amazonian tropical forests. *Agric For Meteorol* 88 (1), 259–268. [https://doi.org/10.1016/S0168-1923\(97\)00038-5](https://doi.org/10.1016/S0168-1923(97)00038-5).
- Stoy, P.C., El-Madany, T.S., Fisher, J.B., Gentine, P., Gerken, T., Good, S.P., Klosterhalfen, A., Liu, S., Miralles, D.G., Perez-Priego, O., Rigden, A.J., Skaggs, T.H., Wohlfahrt, G., Anderson, R.G., Coenders-Gerrits, A.M.J., Jung, M., Maes, W.H., Mammarella, I., Mauder, M., Migliavacca, M., Nelson, J.A., Poyatos, R., Reichstein, M., Scott, R.L., Wolf, S., 2019. Reviews and syntheses: turning the challenges of partitioning ecosystem evaporation and transpiration into opportunities. *Biogeosciences* 16 (19), 3747–3775. <https://doi.org/10.5194/bg-16-3747-2019>.
- Sulman, B.N., Roman, D.T., Scanlon, T.M., Wang, L., Novick, K.A., 2016. Comparing methods for partitioning a decade of carbon dioxide and water vapor fluxes in a temperate forest. *Agric For Meteorol* 226–227, 229–245. <https://doi.org/10.1016/j.agrformat.2016.06.002>.
- Sun, X., Wilcox, B.P., Zou, C.B., 2019. Evapotranspiration partitioning in dryland ecosystems: a global meta-analysis of in situ studies. *J Hydrol (Amst)* 576, 123–136. <https://doi.org/10.1016/j.jhydrol.2019.06.022>.
- Thomas, C., Foken, T., 2007. Flux contribution of coherent structures and its implications for the exchange of energy and matter in a tall spruce canopy. *Boundary Layer Meteorol* 123 (2), 317–337. <https://doi.org/10.1007/s10546-006-9144-7>.
- Thomas, C., Martin, J., Goedekede, M., Siqueira, M., Foken, T., Law, B., Loescher, H., Katul, G., 2008. Estimating daytime subcanopy respiration from conditional sampling methods applied to multi-scalar high frequency turbulence time series. *Agric For Meteorol* 148 (8), 1210–1229. <https://doi.org/10.1016/j.agrformat.2008.03.002>.
- Thomas, C., Mayer, J.-C., Meixner, F.X., Foken, T., 2006. Analysis of low-frequency turbulence above tall vegetation using a doppler sodar. *Boundary-Layer Meteorol* 119, 563–587. <https://doi.org/10.1007/s10546-005-9038-0>.
- Thomas, C.K., Law, B.E., Irvine, J., Martin, J.G., Pettijohn, J.C., Davis, K.J., 2009. Seasonal hydrology explains interannual and seasonal variation in carbon and water exchange in a semiarid mature ponderosa pine forest in central oregon. *Journal of Geophysical Research: Biogeosciences* 114 (G4). <https://doi.org/10.1029/2009JG001010>.
- Thomas, C.K., Martin, J.G., Law, B.E., Davis, K., 2013. Toward biologically meaningful net carbon exchange estimates for tall, dense canopies: multi-level eddy covariance observations and canopy coupling regimes in a mature douglas-fir forest in oregon. *Agric For Meteorol* 173, 14–27. <https://doi.org/10.1016/j.agrformat.2013.01.001>.
- Wang, W., Smith, J.A., Ramamurthy, P., Baeck, M.L., Bou-Zeid, E., Scanlon, T.M., 2016. On the correlation of water vapor and CO₂: application to flux partitioning of evapotranspiration. *Water Resour Res* 52 (12), 9452–9469. <https://doi.org/10.1002/2015WR018161>.
- Webb, E.K., Pearman, G.I., Leuning, R., 1980. Correction of flux measurements for density effects due to heat and water vapour transfer. *Q. J. R. Meteorolog. Soc.* 106 (447), 85–100. <https://doi.org/10.1002/qj.49710644707>.
- Wei, Z., Yoshimura, K., Wang, L., Miralles, D.G., Jasechko, S., Lee, X., 2017. Revisiting the contribution of transpiration to global terrestrial evapotranspiration. *Geophys Res Lett* 44 (6), 2792–2801. <https://doi.org/10.1002/2016GL072235>.
- White, W.A., Alsina, M.M., Nieto, H., McKee, L.G., Gao, F., Kustas, W.P., 2018. Determining a robust indirect measurement of leaf area index in California vineyards for validating remote sensing-based retrievals. *Irrigation Science*. <https://doi.org/10.1007/s00271-018-0614-8>.
- Wichura, B., Ruppert, J., Riederer, M., Foken, T., 2017. Isotope Fluxes. In: T., F. (Ed.), *Energy and Matter Fluxes of a Spruce Forest Ecosystem*. Ecological Studies (Analysis and Synthesis). Springer, pp. 209–245.
- Wilson, K.B., Meyers, T.P., 2001. The spatial variability of energy and carbon dioxide fluxes at the floor of a deciduous forest. *Boundary Layer Meteorol* 98 (3), 443–473.
- Wohlfahrt, G., Gu, L., 2015. The many meanings of gross photosynthesis and their implication for photosynthesis research from leaf to globe. *Plant, Cell & Environment* 38 (12), 2500–2507. <https://doi.org/10.1111/pce.12569>.
- Xu, L., Baldocchi, D.D., Tang, J., 2004. How soil moisture, rain pulses, and growth alter the response of ecosystem respiration to temperature. *Global Biogeochem Cycles* 18 (4). <https://doi.org/10.1029/2004GB002281>.
- Zahn, E., Chor, T.L., Dias, N.L., 2016. A simple methodology for quality control of micrometeorological datasets. *American Journal of Environmental Engineering* 6 (4A), 135–142. <https://doi.org/10.5923/s.ajee.201601.20>.
- Zhou, S., Yu, B., Zhang, Y., Huang, Y., Wang, G., 2016. Partitioning evapotranspiration based on the concept of underlying water use efficiency. *Water Resour Res* 52 (2), 1160–1175. <https://doi.org/10.1002/2015WR017766>.